PLOS ONE

RESEARCH ARTICLE

c-Src functionality controls self-renewal and glucose metabolism in MCF7 breast cancer stem cells

Víctor Mayoral-Varo[1☯], Annarica Calcabrini[1☯¤a], María Pilar Sánchez-Bailón[1☯¤b], Óscar H. Martínez-Costa[1], Cristina González-Páramos[1], Sergio Ciordia[2], David Hardisson[3,4,5], Juan J. Aragón[1], Miguel Ángel Fernández-Moreno[1,6,7], Jorge Martín-Pérez[1,5]*

1 Instituto de Investigaciones Biomédicas A. Sols (CSIC/UAM), Madrid, Spain, **2** Servicio de Espectrometría de Masas, Centro Nacional de Biotecnología (CSIC), Madrid, Spain, **3** Servicio de Anatomía Patológica, Hospital Universitario La Paz, Madrid, **4** Departamento de Anatomía Patológica, Facultad de Medicina, Universidad Autónoma de Madrid (UAM), Madrid, Spain, **5** Instituto de investigaciones sanitarias del hospital La Paz (IdiPAZ), Madrid, Spain, **6** Centro de Investigación Biomédica en Red en Enfermedades Raras (CIBERER), Facultad de Medicina, Universidad Autónoma de Madrid, Madrid, Spain, **7** Instituto de Investigación Sanitaria Hospital 12 de Octubre (imas12), Madrid, Spain

☯ These authors contributed equally to this work.
¤a Current address: National Center for Drug Research and Evaluation, Istituto Superiore di Sanità, Rome, Italy.
¤b Current address: Max Delbrück Center for Molecular Medicine (MDC), Berlin, Germany.
* jorge.martin.perez@csic.es, jmartin@iib.uam.es

Citation: Mayoral-Varo V, Calcabrini A, Sánchez-Bailón MP, Martínez-Costa ÓH, González-Páramos C, Ciordia S, et al. (2020) c-Src functionality controls self-renewal and glucose metabolism in MCF7 breast cancer stem cells. PLoS ONE 15(7): e0235850. https://doi.org/10.1371/journal.pone.0235850

Editor: Antimo Migliaccio, Universita degli Studi della Campania Luigi Vanvitelli, ITALY

Received: March 2, 2020

Accepted: June 23, 2020

Published: July 16, 2020

Peer Review History: PLOS recognizes the benefits of transparency in the peer review process; therefore, we enable the publication of all of the content of peer review and author responses alongside final, published articles. The editorial history of this article is available here: https://doi.org/10.1371/journal.pone.0235850

Data Availability Statement: Data have been uploaded to Proteome Xchange database (Project

Abstract

Deregulation of Src kinases is associated with cancer. We previously showed that SrcDN conditional expression in MCF7 cells reduces tumorigenesis and causes tumor regression in mice. However, it remained unclear whether SrcDN affected breast cancer stem cell functionality or it reduced tumor mass. Here, we address this question by isolating an enriched population of Breast Cancer Stem Cells (BCSCs) from MCF7 cells with inducible expression of SrcDN. Induction of SrcDN inhibited self-renewal, and stem-cell marker expression (Nanog, Oct3-4, ALDH1, CD44). Quantitative proteomic analyses of mammospheres from MCF7-Tet-On-SrcDN cells (data are available via ProteomeXchange with identifier PXD017789, project DOI: 10.6019/PXD017789) and subsequent GSEA showed that SrcDN expression inhibited glycolysis. Indeed, induction of SrcDN inhibited expression and activity of hexokinase, pyruvate kinase and lactate dehydrogenase, resulting in diminished glucose consumption and lactate production, which restricted Warburg effect. Thus, c-Src functionality is important for breast cancer stem cell maintenance and renewal, and stem cell transcription factor expression, effects linked to glucose metabolism reduction.

Introduction

Mammary gland stem cells are capable of self-renewal and to generate all differentiated progeny of the gland [1, 2]. Because of their long lifespan, they can accumulate mutations to become breast cancer stem cells (BCSCs). BCSCs are slow dividing and represent 1–2% of a

accession number: PXD017789, project DOI: 10.6019/PXD017789).

Funding: This work has been supported by grand SAF2016–75991-R (MINECO, AEI/FEDER, UE) to Jorge Martín-Pérez and ISCIII [grand PI 16/00789] to Miguel Ángel Fernández-Moreno. Víctor Mayoral-Varo was supported by the grand SAF2016–75991-R (MINECO, AEI/FEDER, UE). We acknowledge support for publication fee by the CSIC Open Access Publication Support Initiative through its Unit for Information Resources for Research (URICI).

Competing interests: The authors have declared that no competing of interests exist.

tumor biopsy; nevertheless, they reproduce the tumor upon transplantation in nude mice [3]. Breast tumors exhibiting basal phenotype, like the triple negative breast cancers (TNBC), are usually highly metastatic with poor prognosis, resistance to chemotherapy, and are similar to the earliest mammary gland progenitor cells, supporting the hypothesis that therapeutic failure results from inefficient BCSCs targeting [4]. In contrast, luminal A human mammary epithelial cells produce tumors in a hormone-dependent manner. As they express estrogen and progesterone receptors, but not HER2 (human epidermal growth factor 2), and they are poorly /non-metastatic, the MCF7 cell line is a cellular model representative of this type of mammary tumors [5].

The Src-family tyrosine kinases (SFKs) acts as intracellular mediators for signaling pathways from growth factors, estrogen and cytokine receptors activation, etc., mediating pathways involved in proliferation, survival, differentiation, adhesion, migration, and invasion [6–8]. SFKs is overexpressed and/or aberrantly activated in human tumors [7, 9, 10]. In breast cancer, SFKs has been associated with induction, progression, and metastasis [8, 11–16]. c-Src has been involved in glycolysis regulation and Warburg effect [17–20], which is the elevated rate of glycolysis and lactate production in aerobic conditions by tumor cells [21]. As initially shown, c-Src/v-Src phosphorylates several glycolytic enzymes, including enolase and lactate dehydrogenase (LDH) [22]. In 3T3 fibroblast, v-*src* transfection leads to increased expression of glucose uptake [23]. c-Src phosphorylates Y10-LDH, increasing its activity, which promotes invasion, anoikis resistance, and metastasis of breast cancer cells [19]. Similarly, c-Src phosphorylates hexokinase 1 and 2 (HK1, HK2) augmenting their activity, which stimulates glycolysis, cell proliferation, migration, invasion, and tumorigenesis [20]. In human glioblastoma U87 and U251 cells, EGFR activation leads to c-Src stimulation and subsequent Y59-Cdc25A phosphorylation, which dephosphorylates pyruvate kinase (PKM2), promoting its interaction with β-catenin, its transactivation and Myc transcription that induces Glut-1 (glucose transporter 1), PKM2 and LDHA expression and, consequently, the Warburg effect and tumorigenesis [18].

We previously showed in MCF7 cells that conditional Tet-On expression of SrcDN (Src-Dominant Negative) leads to inhibition of proliferation, attachment, spreading and migration in cultured cells. Inoculation of cells in nude mice generates tumors, while induction of SrcDN expression significantly reduces their tumorigenesis, and causes regression when induced in established tumors [24]. The Src-DN is a chicken paralog of c-Src with two mutations (c-Src-K295M/Y527F). The mutation K295M prevent binding of ATP to c-Src, avoiding its tyrosine kinase activity, the second point mutation Y527F at the C-terminal of the molecule, that is phosphorylated by CSK (C-terminal Src Kinase), provokes that c-Src is forced to maintain its open conformation, which implies full functionality of the SH2 and SH3 domains [6–8].

Here we addressed the question as to whether interfering SFKs functionality by SrcDN expression directly affects MCF7-BCSC renewal. Thus, here we isolate by FACS the enriched population of BCSCs (ESA^+-$CD44^+$-$CD24^{-/Low}$ cells, from now on $CD24^-$) and the so-called tumor-differentiated cells (ESA^+-$CD44^+$-$CD24^+$ cells, from now on $CD24^+$) from MCF7-Tet-On-SrcDN [24], and test their capacity of self-renewal. Our findings show that c-Src is important for mammospheres self-renewal, which is associated with an alteration in glucose metabolism.

Materials and methods

Reagents

Information about antibodies used in these experiments is in S2 Table in S1 File (Antibodies). BCA protein assay (Termofisher); Acrylamide/bis 40% solution, 29:1 (3.3% C), ammonium

persulfate and clarity immunoblot ECL substrate (Bio-Rad); trypan blue, doxycycline (Doxy), BSA, puromycin, and insulin (Sigma-Aldrich); EGF, and bFGF (PeproTech EC Ltd., London, UK); G418, versene, and trypsin (Invitrogen); tetracycline-free fetal bovine serum (Tet-Free-FCS, PAA Laboratories GmbH). Other chemical reagents and enzymes used were of analytical grade and purchased from Roche, GE Healthcare, or Sigma-Aldrich/Merck.

Cells and culture

MCF7 (HTB-22) were from ATCC. Cells were mycoplasma free and authenticated by short-tandem-repeat analysis (GenePrintR 10 System from Promega, and GeneMapper v3.7 STR profile analysis software, Life Technologies) (see Supplementary Information). Profiles obtained were checked against public databases ATCC and DSMZ. MCF7-Tet-On-SrcDN cells bearing a Doxy-inducible SrcDN (avian c-Src-K295M/Y527F) were previously generated [24] and maintained in DMEM, 5% Tet-Free-FCS, 2 mM glutamine, 100 IU/mL penicillin, 100 μg/mL streptomycin, and 0.2 mg/mL G418, 0.5 μg/mL puromycin for selection.

Isolation and culture of $CD24^-$ and $CD24^+$ subpopulations from MCF7 cells

The enriched subpopulations of $CD24^-$ and $CD24^+$ cells derived from MCF7-Tet-On-SrcDN were isolated by fluorescence-activated cell sorting (FACS), as described [3]. Briefly, $1x10^7$ cells were detached from the culture plates with versene (5 min, 37˚C), and then simultaneously labeled with antibodies to ESA-FITC, CD44-APC, CD24-PE, and with their respective isotypic immunoglobulins. Cells were washed and subjected to FACS with a FACS-Vantage cell sorter (BD, San Jose CA) equipped with an argon ion laser (emission at 488 nm) and a He-Ne laser (emission at 633 nm). Cells were gated on forward and side scatters properties and specific fluorescent signals were collected using 530 nm (FITC), 575 nm (PE) and 660 nm (APC) bandpass filters. About 1.6% of the cell population showed the $CD24^-$ (ESA^+-$CD44^+$-$CD24^-$) phenotype and were isolated. In parallel, the $CD24^+$ (ESA^+-$CD44^+$-$CD24^+$) cells were also isolated as described [3].

$CD24^-$ cells were maintained in mammosphere media (1:1 DMEM/HAM'S F12, 2 mM glutamine, 100 IU/mL penicillin, 100 mg/mL streptomycin, 5 μg/mL Insulin, 20 ng/mL EGF, 10 ng/mL bFGF, 4 mg/ml BSA), and 0.2 mg/mL G418, 0.5 μg/mL puromycin to maintain selection for c-SrcDN expression [24], and they were grown in suspension in 6-multiwell ultralow attachment plates (Falcon 351146, BD); $CD24^+$ cells were cultured in DMEM, 5% Tet-Free-FCS, 2 mM glutamine, 100 IU/mL penicillin, 100 mg/mL streptomycin, and 0.2 mg/mL of G418 and 0.5 μg/mL puromycin in standard plates (Falcon, BD). Also, another protocol was employed for BCSCs enrichment to enrich for BCSCs from MCF7-Tet-On-SrcDN, single cells obtained after trypsinization of adherent cultures were plated at $1x10^3$ cells/mL and cultured as described above for $CD24^-$ [25].

Sphere Formation Efficiency (SFE)

SFE from MCF7-Tet-On-SrcDN was determined as described [26]. Briefly, single cell suspensions of adherent cultures were plated in 6-well ultralow attachment plates (Falcon, Corning Life Science) at $2x10^3$ cells/well and maintained in serum-free DMEM/F12 media (1:1), BSA (4 mg/mL), EGF (20 ng/mL) and bFGF (20 ng/mL), insulin (5 μg/mL), hydrocortisone (5 μg/mL) to obtain mammospheres. Fifteen days later, mammospheres were dissociated into single cells that were plated in 6-well ultralow attachment plates at $2x10^3$ cells/well in mammosphere culture media, 3 wells without Doxy (Control) and 3 wells with Doxy (2 μg/mL). During the experiments Doxy was renewed every 3 days in cultures. Each mammosphere generation was

cultured about 15 days. Mammospheres (sphere-like structures with diameter $\geq$ 50 μm) were clearly detected by optical phase contrast microscope (Nikon-Eclipse TS100, 4x magnification). For mammosphere dissociation, they were collected in a sterile tube and allow them to sediment, the media was removed with a pipette and trypsinized in Tris-Saline pipetting up and down to facilitate mammosphere dissociation, cells were then collected by centrifugation to remove trypsin, washed with mammosphere media and counted. Single cells were seeded again for mammosphere formation in 6-well ultralow attachment plates at $2x10^3$ cells/well. The experiment ended at 3rd generation of mammosphere formation. The cells were growth in absence (Control) or presence (Doxy) of 2 μg/ml Doxy for three generations, and renewed every three days. SFE was calculated as number of spheres formed per number of seeded cells and expressed as % means ± SD. The SFE experiments were repeated 5 times, each one of them was carried out in triplicates ($p<0.05^*$).

Immunohistochemistry of mammospheres

Mammospheres derived from MCF7-Tet-On-SrcDN were fixed in 4% formaldehyde solution. Fixed samples were paraffin embedded, and 5 μm sections were analyzed by hematoxylin/eosin, and E-cadherin and P-cadherin staining were performed using Envision method [27].

Immunoblotting analysis

Preparation of cell lysates from mammospheres and immunoblotting analyses were carried out as previously described [24]. Briefly, mammospheres were collected by centrifugation at 200xg 5 min at room temperature, washed twice with cool PBS and lysed at 4˚C with lysis buffer [10 mM Tris–HCl (pH 7.6), 50 mM NaCl, 30 mM sodium pyrophosphate, 5 mM EDTA, 5 mM EGTA, 0.1% SDS, 1% Triton X-100, 50 mM NaF, 0.1 mM Na_3VO_4, 1 mM PMSF, 1 mM benzamidine, 1 mM iodoacetamide and 1 mM phenantroline]. Cell lysates were obtained by centrifugation at 21,380xg for 30 min at 4˚C; protein concentration in the supernatant was determined by BCA protein assay (Pierce, Rockford, IL), and lysates were adjusted to equivalent concentrations with lysis buffer. Aliquots of 10–40 μg of total cell lysate were then separated on SDS–PAGE. Proteins were transferred to PVDF membranes that were blocked overnight at 4˚C with 5% non-fat milk in TTBS (TBS with 0.05% Tween-20). Incubation with primary specific antibodies was carried out overnight at 4˚C, and horseradish peroxidase-conjugated secondary antibodies in blocking solution for 1 h at room temperature. Immunoreactive bands were visualized by ECL kit.

Quantitative proteomic analysis

Briefly, MCF7-Tet-On-SrcDN derived mammospheres at 3rd generation from two independent experiments cultured either in the absence (Control) or presence of Doxy (2 μg/mL) were collected by centrifugation, washed with PBS, and lysed in 9 M urea, 2 M thiourea, 5% CHAPS, and 2 mM TCEP. The samples were precipitated by methanol/chloroform and quantified by Pierce 660nm Protein Assay. Then 30 μg of protein from each sample were trypsinized, and the resulting peptides were labeled using iTRAQ 4-plex reagent (SCIEX, Foster City, CA, USA) according to the manufacturer's instructions and named as follows: Control-1, 114-tag; Doxy-1, 115-tag; Control-2, 116-tag; Doxy-2, 117-tag. Samples were pooled, evaporated to dryness and frozen. The pool was separated into 5 fractions in a reverse phase C18 chromatography at basic pH and cleaned with a StageTip-C18. The 5 fractions were quantified by fluorimetry, and 1 μg of each fraction was separated by C-18 reverse phase chromatography during 150 min. The eluted peptides passed then into 5600 Triple-TOF MS (SCIEX, Foster City, CA). The raw data of the combined 5 fractions was exported to the search-engine Mascot

Server v2.5.1 (Matrix Science, London, UK) confronted to the *Homo sapiens* UniProt database. Peptide mass tolerance was set to ± 25 ppm for precursors and 0.05 Da for fragment masses. Frequency distribution histograms of protein ratios were obtained into Excel 2010. Log2 peptide ratios followed a normal distribution that was fitted using least squares regression. Mean and standard deviation values derived from the Gaussian fit were used to calculate p-values and quantification of False Discovery Rates (FDR). The confidence interval for protein identification was set to $\geq$ 95% ($p<0.05$) and only peptides with an individual ion score above the 1% False Discovery Rates (FDR) threshold were considered correctly identified. Only proteins having at least two quantitated peptides were considered in the quantitation. A 5% quantitation FDR threshold was estimated to consider the significant differentially expressed proteins.

The mass spectrometry proteomics data have been deposited to the ProteomeXchange Consortium via the PRIDE [28] partner repository (Project accession number: PXD017789, project DOI:10.6019/PXD017789).

Enzymatic activity assays

Mammospheres at 3rd generation derived from MCF7-TET-ON-SrcDN cells were seeded into a six-well plate and cultured with fresh medium -/+ Doxy (2 μg/mL) for 12–24 h. Cells were harvested by centrifugation, washed twice with PBS and preincubated for 10 min in PBS. Then, cells were collected by centrifugation, suspended in fresh culture medium and incubated for another 4 h. Cells were harvested by centrifugation at room temperature at 0 and 4 h incubation and treated with 200 μL lysis buffer (Tris-HCl (pH 7.5), 1 mM EDTA, 0.5 mM dithiothreitol, 0.2% Triton X-100, 0.2 mg/mL deoxycholate, 0.2 mM phenylmethylsulfonyl fluoride, and 2.5 μg/mL leupeptin), and homogenized at 4˚C by pipetting up and down. The homogenate was centrifuged at 21,380x*g* for 15 min at 4˚C and the supernatant was used for enzymatic activity measurements. Hexokinase (HK) activity was determined spectrophotometrically at 340 nm by following the G6PDH dependent conversion of NADP to NADPH. The assay mixture contained 100 mM Tris-HCl (pH 8.0), 0.5 mM EDTA, 10 mM $MgCl_2$, 5 mM MgATP, 2 mM glucose, 0.5 mM $NADP^+$ and 10 U/mL glucose 6-phosphate dehydrogenase (G6PDH) in a final volume of 1 mL. HK activities were calculated according to the slope of the resulting curves in the log phase. The initial velocity of lactate dehydrogenase (LDH) was determined by measuring spectrophotometrically the NADH consumption at 340 nm in a 1 mL reaction mixture (50 mM HEPES pH 7.2, 100 mM KCl, 5 mM $MgCl_2$, 0.15 mM NADH, and 2 mM pyruvate). The slopes of the initial linear decrease were used to calculate initial velocities. Pyruvate kinase (PK) activity was measured by following the production of pyruvate. The reaction mixture consisted of 50 mM HEPES (pH 7.2), 100 mM KCl, 5 mM $MgCl_2$, 0.15 mM NADH, 1 mM MgADP, 2 mM phosphoenolpyruvate, and 1 U/mL of LDH as the auxiliary enzyme in a final volume of 1 mL. PK activity was determined spectrophotometrically as above by recording the change of 340 nm absorbance produced by NADH oxidation. One unit of enzyme activity is defined as the amount of enzyme catalyzing the conversion of 1 μmol of substrate/min at 25˚C. Enzymatic activities of different samples were normalized against the corresponding protein concentrations in the lysates.

Lactate production and glucose consumption assays

Cells were treated as above. At 0 and 4 h incubation, cells were harvested by centrifugation at room temperature, and the culture medium was removed and stored at -70˚C for lactate production and glucose consumption measurements. Cell pellets were homogenized in ice-cold 8% (v/v) perchloric acid in 40% ethanol. After centrifugation at 21,380x*g* for 15 min at 4˚C, the supernatant was neutralized to pH 7.0 with a 2 M KOH and 0.5 M triethanolamine solution,

the mixture was incubated on ice for 15 min, and precipitated $KClO_4$ was removed by centrifugation. Glucose and lactate content in culture medium and levels of intracellular lactate were assessed by using standard enzymatic techniques [29]. Briefly, lactate was determined in a reaction containing 0.5 M Glycine, 0.2 M hydrazine, 3.4 mM EDTA, 1.5 mM NAD^+, and 10 U/mL of LDH, pH 9.5. The reaction mixture for glucose measurement consisted of 0.1 M triethanolamine, 5 mM $MgCl_2$, 0.5 mM $NADP^+$, 1 mM ATP, 1 U/mL hexokinase and 3 U/mL G6PD, pH 7.4. The function of the glycolytic pathway was evaluated by the amount of lactate produced per hour after 4 h incubation. Glucose consumption rate (per hour) was calculated considering the difference between the amount in the medium at 0 h and that recovered in the medium after 4 h incubation. Glucose and lactate content were normalized to the protein concentration of cells cultured under similar conditions and obtained as described above for enzymatic activity.

Oxygen consumption and determination of ATP concentration

Mammospheres at 3rd generation cultured in the absence or presence of 2 μg/mL Doxy were dissociated to single-cell suspension as for SFE, resuspended in mammospheres media with or without pyruvate and without BSA to 10^6 cells/mL and the oxygen consumption of $2x10^6$ cells was measured by high-resolution respirometry with the OROBOROS oxygraph-2k in a standard configuration, at 37˚C and a 750-rpm stirrer speed as described [30]. The protocol includes the determination in a sequential manner of the aerobic metabolic activity under routine culture conditions with the physiological substrates in culture medium (Cr), the oligomycin-inhibited leak rate of respiration after inhibition of ATP synthase with 2 μg/mL oligomycin (CrO) and the maximum respiratory capacity of uncoupled mitochondria in non-permeabilized cells (CrU), obtained by sequential addition of 0.5 μM boluses of trifluoro-carbonylcyanide phenylhydrazone (FCCP). The protonophore FCCP dissipates the proton inner membrane gradient making ETC to function at its maximal rate since oxygen and protons are not limiting for the ETC Complex IV catalysis. All values, including physiological conditions and the maximal respiratory capacity, are derived by subtracting non- mitochondrial respiration from the FCCP rate.

Measurements of total ATP concentration were made in mammospheres that were maintained for at least 15 days -/+ Doxy (2 μg/mL) at 0 and 4 h, as previously described [31], following instructions of the ATP Bioluminescence Assay Kit CLS II (Roche, Ref. 11699695001).

Statistical analyses

Mean values, standard deviation and statistical significance between data from two different experimental conditions were determined by two-tail Student *t*-test. In all figures, data represent the Mean from at least three separate biological repeats done in at least triplicates each ± SD (standard deviation), $^*p < 0.05$, $^{**}p < 0.01$, and $^{***}p < 0.001$.

Results

Isolation and characterization of an enriched population of BCSCs from MCF7 cells

To determine the role of SrcDN in the self-renewal of the enriched subpopulation of BCSCs, we isolated $CD24^-$ (ESA^+-$CD44^+$-$CD24^-$) and $CD24^+$ (ESA^+-$CD44^+$-$CD24^+$) cell populations derived from MCF7-Tet-On-SrcDN by FACS. Cells were first sorted as ESA^+ and then for being $CD44^+$-$CD24^-$ (1.6%), while the $CD44^+$-$CD24^+$ represented 98.4% of total cell population (Fig 1A, isotype controls shown in S1 Fig in S1 File). $CD24^-$ cells formed mammospheres

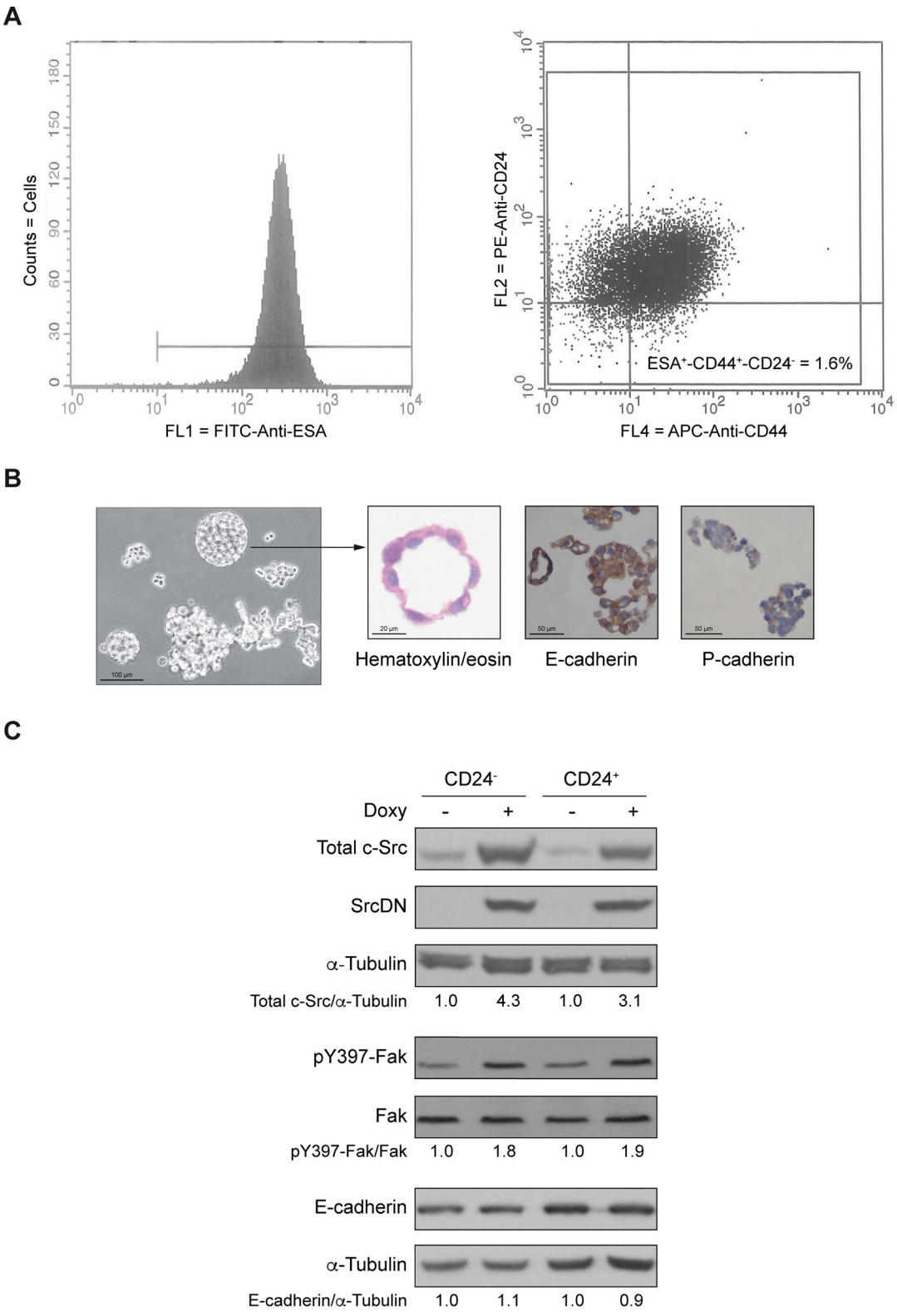

Fig 1. Cell sorting of CD24$^-$ and CD24$^+$ subpopulations of MCF7 cells. (A) Histograms of ESA-FITC positive cells that were later sorted for CD44-APC positive and CD24-PE negative (1.6%). (B) Microphotograph under light microscope of mammospheres from CD24$^-$ cells in culture. Representative images of spheres stained with hematoxylin/eosin, E-cadherin or P-cadherin. Scales bars are included. (C) Immunoblot of total c-Src, SrcDN, p-Y397-Fak/Fak, and E-cadherin, using α-Tubulin

expression as loading control from CD24$^-$ cells forming mammospheres and CD24$^+$ cells in absence (Control) or presence of Doxy (2 μg/mL) for induction of SrcDN during three passages. The ratios of the proteins Total c-Src, SrcDN, and E-cadherin with the loading control α-Tubulin, or pY397-Fak/Fak were calculated and referred to -Doxy (Control) considered as 1. These are representative results from 3 independent experiments.

https://doi.org/10.1371/journal.pone.0235850.g001

(Fig 1B) that after staining with hematoxylin/eosin showed a monolayer cell-structure with their nuclei oriented towards the lumen. Furthermore, mammospheres expressed E-cadherin, but not P-cadherin (Fig 1B). These results suggested that both CD24$^-$ (mammospheres) and CD24$^+$ cells maintained the epithelial phenotype of the MCF7 total population.

To determine the functionality of SrcDN, protein extracts from mammospheres from CD24$^-$ and from CD24$^+$ cell subpopulations were blotted for pY397-Fak, showing an increased phosphorylation upon SrcDN induction. This is consistent with previous results showing that SH2 domain from SrcDN binds pY397-Fak protecting from dephosphorylation [24, 32, 33], and with the reduction of pY925-Fak, p-Y-p130CAS, pY118-Paxillin phosphorylation by c-Src in MCF7 cells [24]. Expression of E-cadherin remained unaltered in CD24$^-$ and CD24$^+$ upon SrcDN induction (Fig 1C). SrcDN expression was tested by detecting total c-Src and avian SrcDN (Fig 1C).

c-Src functionality is necessary for mammospheres self-renewal

To characterize the role of c-Src in the enriched subpopulation of BCSC self-renewal, we analyzed whether induction of SrcDN expression altered formation of mammospheres from MCF7-Tet-On-SrcDN. Self-renewal capacity was confirmed by three successive generations of mammospheres, where a progressive enrichment of mammosphere-forming cells (CD24$^-$) was observed (S2 Fig in S1 File). Then, we determined Sphere Formation Efficiency (SFE) upon induction of SrcDN expression from the first generation and found that it significantly reduced SFE as compared to control (-Doxy) at the 3rd generation (Fig 2A). This effect was

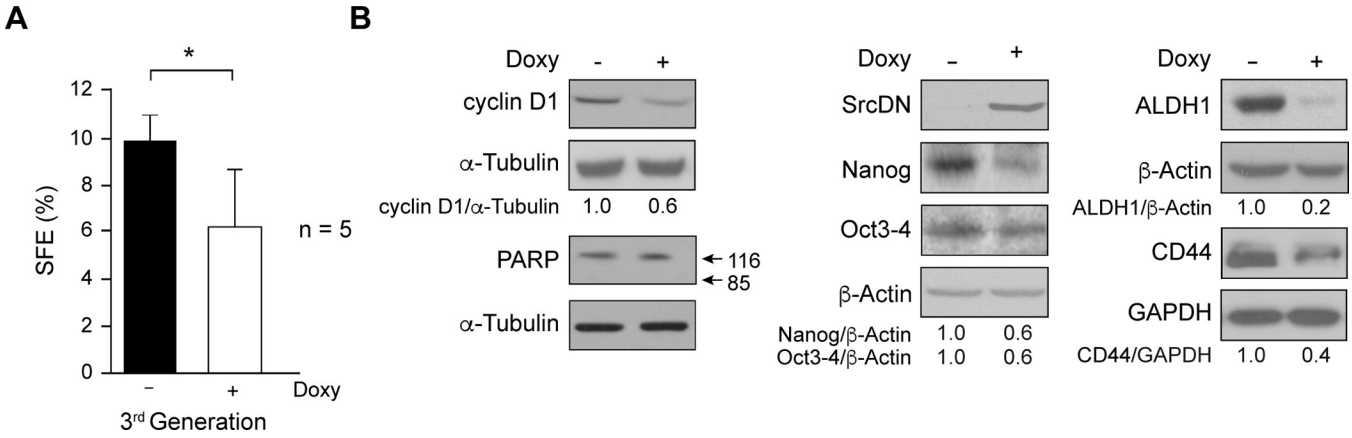

Fig 2. Self-renewal of mammospheres derived from MCF7. (A) The Sphere Formation Efficiency (SFE) was determined in MCF7-Tet-On-SrcDN. Thus, single cell suspensions from adherent cells were plated in 6-well ultralow attachment plates at 2x10^3 cells/well and cultured in mammosphere medium. Fifteen days later, mammospheres were dissociated into single cells that were divided into two groups: Control (-Doxy) and Doxy treated (2 μg/mL). Doxy-treatment was maintained for three generations, and renewed every 3 days. SFE at 3rd generation was calculated as number of spheres formed per number of seeded cells and expressed as % means ± SD. The SFE experiments were repeated 5 times, each one of them was carried out in triplicates. ($p<0.05^*$). (B) Total cell extracts from the 3rd generation of mammospheres treated as above (panel A) were used to determine by immunoblotting expression of cyclin D1, PARP, with α-Tubulin, as a loading control, and SrcDN, Nanog, Oct3/4, ALDH1, and CD44, employing GAPDH or β-Actin, as a loading control. The net quantification of the gel bands after subtracting the background was carried out with ImageJ program and expressed in arbitrary units. These are representative results from 3 independent experiments. The ratios of the proteins SrcDN, Nanog, Oct3/4, ALDH1, and CD44 and their loading controls GAPDH or ß-Actin, or pY10-LDHA/LDHA were calculated and referred to -Doxy (Control) considered as 1.

https://doi.org/10.1371/journal.pone.0235850.g002

clearly evident from the 1st generation (S2 Fig in S1 File), although no morphological alterations were observed upon SrcDN induction (data not shown). Consistently, cyclin D1 expression at the 3rd generation was also reduced. However, SrcDN expression did not appear to cause apoptosis, as PARP degradation was undetectable. To determine the nature of cells that form mammospheres, we have dissociated mammospheres at the 3rd generation, labelled cells with anti-CD24-PE and CD44-APC monoclonal antibodies, as well as with isotypic immunoglobulins for control, and analyzed them by flow cytometry. S3 Fig in S1 File showed that in control mammospheres most of cells are $CD44^{+}$-$CD24^{-}$. In contrast, in Doxy-treated mammospheres a large number of cells were $CD44^{+}$-$CD24^{+}$. In addition, the analysis of the expression level of these markers (MFC, mean fluorescence channel) indicates that, along with an increase of expression of CD24, treated mammospheres show a reduced expression of CD44. Moreover, expression of pluripotency-related transcription factors involved in self-renewal Nanog, Oct3/4, and stem cell markers ALDH1, and CD44 [34–36] were also reduced (Fig 2B). Together, these results suggested that c-Src functionality is relevant for MCF7-mammosphere renewal.

Proteomic analyses of mammospheres

Since c-Src functionality is important for SFE of MCF7-mammospheres, we analyzed whether SrcDN induction quantitatively modified protein expression. Proteomic analyses identified 2,759 proteins with at least two peptides, full data available at Proteome Xchange database (project accession number: PX017789, project DOI: 10.6019/PX017789). From those, only 101 proteins were differentially expressed with an FDR < 5% (S1 Table in S1 File). In the Fig 3 only proteins having at least two quantitated peptides and <5% quantitation FDR with the same tendency in both experiments were included. Thus, induction of SrcDN by Doxy (2 μg/mL) diminished the levels of fifteen proteins, and increased the levels of four of them (Fig 3, and S4 Fig in S1 File). The most increased protein in Doxy/Control is c-Src, which most likely should correspond to SrcDN induced by Doxy-treated mammospheres, as the identity of *Homo Sapiens* and *Gallus-Gallus* c-Src at the amino acid sequences is 94%. Results obtained were submitted to GSEA and found that glycolysis was significantly reduced in MCF7-mammospheres upon SrcDN induction (S5 Fig in S1 File), which was consistent with data from Fig 3.

DIFFERENTIAL PROTEINS FOR 5% FDR AT QUANTITATION LEVEL		Doxy-18/Control-18			Doxy-29/Control-29		
Protein_AC	Description	Ratio	Log2	FDR	Ratio	Log2	FDR
O14737	Programmed cell death protein 5 OS=Homo sapiens GN=PDCD5 PE=1 SV=3	#N/A	#N/A	#N/A	#N/A	#N/A	#N/A
P00338	L-lactate dehydrogenase A chain OS=Homo sapiens GN=LDHA PE=1 SV=2	0.589	-0.764	2.36%	0.567	-0.818	0.04%
P00558	Phosphoglycerate kinase 1 OS=Homo sapiens GN=PGK1 PE=1 SV=3	0.583	-0.777	2.05%	0.569	-0.813	0.04%
P05161	Ubiquitin-like protein ISG15 OS=Homo sapiens GN=ISG15 PE=1 SV=5	0.540	-0.889	0.54%	0.337	-1.568	0.00%
P09104	Gamma-enolase OS=Homo sapiens GN=ENO2 PE=1 SV=3	0.541	-0.885	0.56%	0.642	-0.639	0.94%
P09972	Fructose-bisphosphate aldolase C OS=Homo sapiens GN=ALDOC PE=1 SV=2	0.569	-0.812	1.37%	0.612	-0.708	0.31%
P13674	Prolyl 4-hydroxylase subunit alpha-1 OS=Homo sapiens GN=P4HA1 PE=1 SV=2	0.572	-0.807	1.41%	0.653	-0.616	1.45%
P18085	ADP-ribosylation factor 4 OS=Homo sapiens GN=ARF4 PE=1 SV=3	0.494	-1.017	0.09%	0.684	-0.549	4.15%
P19525	Interferon-induced, double-stranded RNA-activated protein kinase OS=Homo sapiens GN=EIF2AK2 PE=1 SV=2	0.571	-0.807	1.43%	0.594	-0.751	0.13%
P52789	Hexokinase-2 OS=Homo sapiens GN=HK2 PE=1 SV=2	0.546	-0.874	0.67%	0.428	-1.226	0.00%
P61006	Ras-related protein Rab-8A OS=Homo sapiens GN=RAB8A PE=1 SV=1	0.585	-0.773	2.14%	0.606	-0.722	0.24%
P84077	ADP-ribosylation factor 1 OS=Homo sapiens GN=ARF1 PE=1 SV=2	0.363	-1.464	0.00%	0.559	-0.838	0.03%
P84085	ADP-ribosylation factor 5 OS=Homo sapiens GN=ARF5 PE=1 SV=2	0.365	-1.452	0.00%	0.497	-1.009	0.00%
Q8N5K1	CDGSH iron-sulfur domain-containing protein 2 OS=Homo sapiens GN=CISD2 PE=1 SV=1	0.567	-0.818	1.36%	0.636	-0.652	0.75%
Q9H299	SH3 domain-binding glutamic acid-rich-like protein 3 OS=Homo sapiens GN=SH3BGRL3 PE=1 SV=1	0.550	-0.862	0.74%	0.454	-1.139	0.00%
P12931	*Proto-oncogene tyrosine-protein kinase Src OS=Homo sapiens GN=SRC PE=1 SV=3*	*3.079*	*1.622*	0.00%	*2.738*	*1.453*	0.00%
P42695	*Condensin-2 complex subunit D3 OS=Homo sapiens GN=NCAPD3 PE=1 SV=2*	*2.595*	*1.376*	0.00%	*2.776*	*1.473*	0.00%
Q3ZCQ8	*Mitochondrial import inner membrane translocase subunit TIM50 OS=Homo sapiens GN=TIMM50 PE=1 SV=2*	*1.769*	*0.823*	4.91%	*1.673*	*0.743*	1.65%
Q93070	*Ecto-ADP-ribosyltransferase 4 OS=Homo sapiens GN=ART4 PE=2 SV=2 CD297*	*2.120*	*1.084*	0.18%	*1.746*	*0.804*	0.59%

Down-expressed
Up-expressed

Significant (FDR<1%)	
Significant (1%<FDR>5%)	

Fig 3. Quantitative proteomic analysis of mammospheres derived from MCF7-Tet-On-SrcDN. The analysis was carried out in two independent experiments from the total cell extract of the 3rd generation mammospheres either untreated (Control) or Doxy-treated. Only proteins having at least two quantitated peptides and <5% quantitation FDR in both experiments are included in the figure.

https://doi.org/10.1371/journal.pone.0235850.g003

Role of c-Src in the regulation of glycolysis in MCF7-mammospheres

As glycolytic pathway was inhibited in mammospheres upon SrcDN induction, we investigated whether glucose consumption was altered, and found that it was significantly reduced in mammospheres expressing SrcDN (Fig 4A), which parallels a reduction in Glut-1 levels (Fig 4D), the major glucose transporter in tumor cells [37]. In cancer cells, Src enhances HK enzymatic activity, a rate-limiting enzyme of glycolysis, by direct phosphorylation [20]. Since SrcDN is a kinase-dead mutant and competes with endogenous Src kinases [38], HK enzymatic activity was significantly inhibited in Doxy-treated mammospheres (Fig 4C). In addition, HK2 levels were also diminished (Fig 4D), supporting proteomic results (Fig 3). However, we were unable to detect HK2 tyrosine phosphorylation. Similarly, PKM enzymatic activity was also inhibited upon SrcDN expression (Fig 4C). In head and neck and in breast cancer cells, Src phosphorylates and enhances LDHA [19]. We tested for SrcDN effects on LDHA enzymatic activity, expression, and phosphorylation. In Doxy-treated mammospheres, LDH activity was significantly reduced (Fig 4C), as it was pY10-LDHA/LDHA ratio (Fig 4D). It is well established that c-Myc and HIF-1 promote the expression of enzymes implicated in glycolysis regulation, including HK2 and LDHA [39, 40, 41]. Thus, we analyzed c-Myc and HIF-1 expression level in Control (Doxy-untreated) and Doxy-treated (2 μg/mL) 3rd mammosphere generations by SYBR Green-q-RT-PCR and by immunoblotting (see Supplementary Material). SrcDN induction did not modify c-Myc expression both at RNA and protein level while HIF-1 RNA expression was significantly reduced. In addition, we were not able to detect HIF-1 protein expression by immunoblotting as the protein is extremely labile (S6 Fig in S1 File). The decrease in glucose consumption was paralleled by a nearly stoichiometric reduction of lactate production (lactate/glucose ratio of 1.45 ± 0.12 and 1.58 ± 0.09 for wild-type and SrcDN-mammospheres, respectively). Thus, the production of lactate from glutaminolysis is very limited. Interestingly, although lactate production diminished, intracellular accumulation of this metabolite was increased (Fig 4B), a result consistent with the reduced expression of MCT-1 (SLC16A1, proton coupled monocarboxylate transporter 1) in Doxy-treated mammospheres (Fig 4D), the major lactate transporter in tumor cells [42].

Effects of SrcDN on oxygen consumption and ATP production

Results showed that SrcDN expression inhibited glycolysis and altered the lactate levels in mammospheres. We next determined the effects of SrcDN in mitochondrial respiration capacity, either in culture without pyruvate, and in normal culture media, which containing saturating concentrations of pyruvate to the uncoupled mitochondria to glycolysis, pushing oxygen consumption to its highest. Basal oxygen consumption of cells dissociated from mammospheres in media containing pyruvate was unmodified by SrcDN expression, while the maximum was significantly inhibited (Fig 5A). Similarly, oxygen consumption carried out in media without pyruvate was also unaltered in basal conditions, but the maximum was highly reduced in mammospheres expressing SrcDN (Fig 5A, and S7 Fig in S1 File: OCR profiles). Furthermore, analyses of ATP production did not differ between cells dissociated from mammospheres expressing SrcDN and control cells (Fig 5B). Neither alteration in ROS level, nor modification of catalase or MnSOD expression was observed upon SrcDN induction in mammospheres, as compared to controls (Doxy-untreated) (S8 Fig in S1 File).

Discussion

Cancer stem cells, which represent only a small subpopulation in a tumor, possess the ability of self-renewal and to form new tumors in nude mice. In breast cancer, BCSCs are defined by expression of ESA, CD44 and low CD24 expression ($ESA^+/CD44^+/CD24^-$), and high

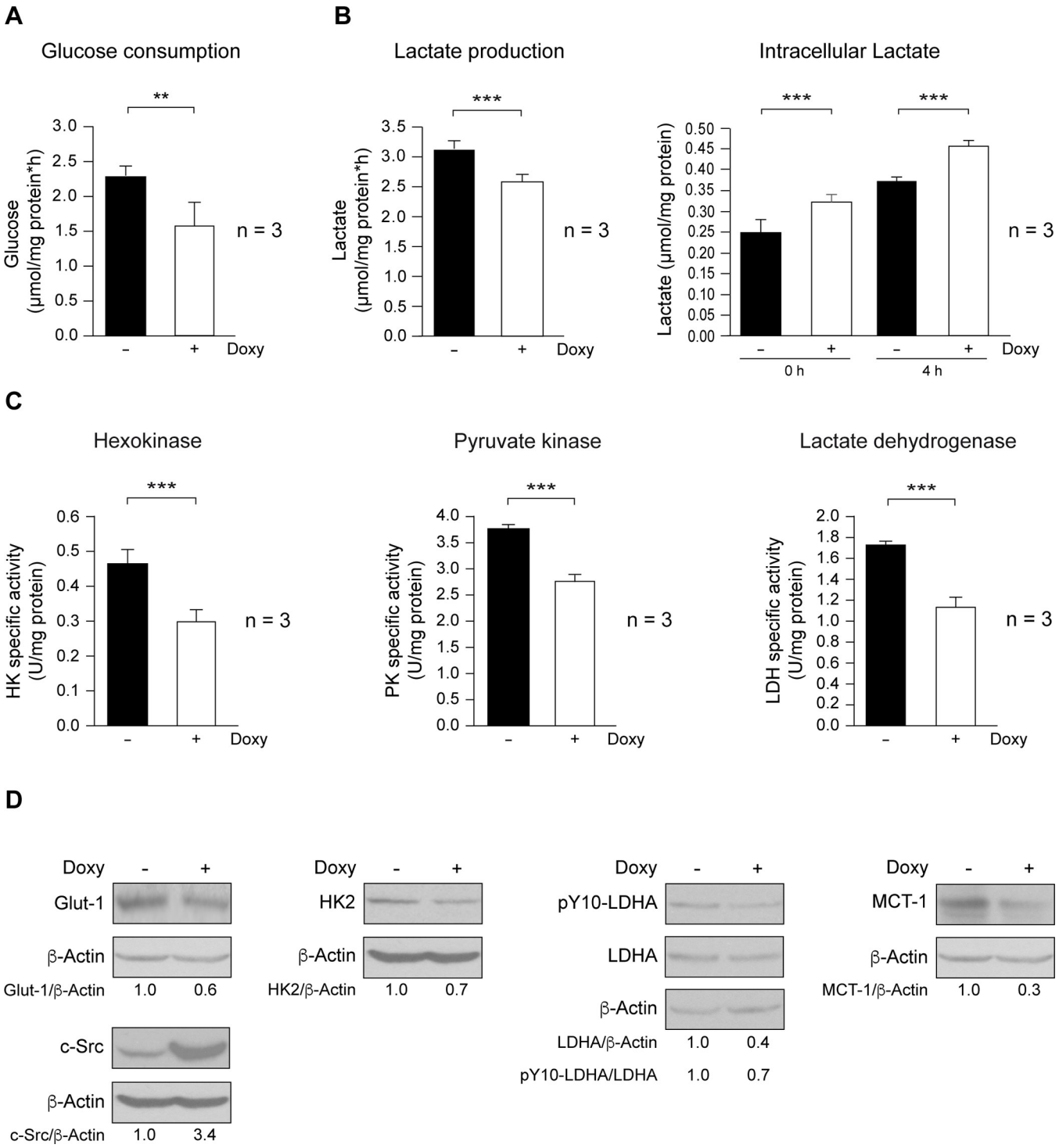

Fig 4. Expression of SrcDN reduced glycolysis in MCF7 mammosphere-derived cells. Control and Doxy-treated (2 μg/mL) mammospheres from the 3rd generation were used to study glycolysis. (A) Determination of glucose consumption. (B) Lactate production, intracellular lactate. (C) Enzymatic activity of hexokinase (HK), pyruvate kinase (PK), lactate dehydrogenase (LDH). (***$p<0.001$). (D) Expression of Glut-1, total c-Src, HK2, pY10-LDHA, LDHA, and MCT-1, was determined by immunoblotting, employing ß-Actin as a loading control. These are representative results from 3 independent experiments. The ratios refer to -Doxy considered as 1.

https://doi.org/10.1371/journal.pone.0235850.g004

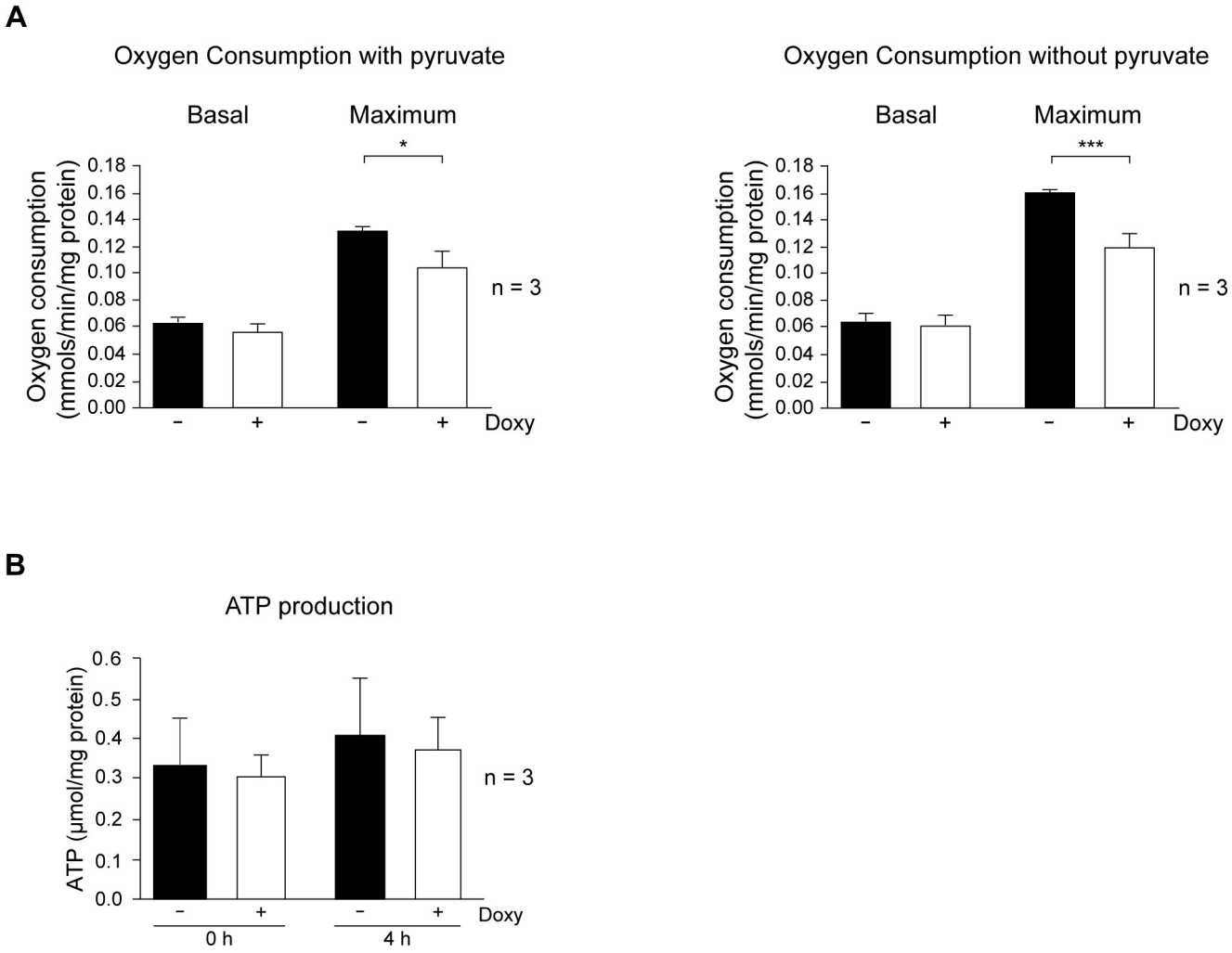

Fig 5. Effects of SrcDN on oxygen consumption, and ATP production in MCF7 mammosphere-derived cells. (A) Oxygen consumption in normal media containing pyruvate or in media without pyruvate and (B) ATP production, they were determined in cells obtained from Control (Doxy-untreated) and Doxy-treated (2 μg/mL) 3rd generation mammospheres.

https://doi.org/10.1371/journal.pone.0235850.g005

tumorigenic capabilities [3]. In this context, the low percentage of BCSCs ($CD24^-$ cells) that we found here, correlates with previous observations [3] and confirms that the isolation of the $CD24^-$ cells was properly done.

In this study we analyzed the effects of the induction of a dominant-negative mutant of the protooncogene c-Src, the SrcDN. We found that disrupting c-Src pathways by induction of SrcDN expression reduced the self-renewal capabilities (SFE) of the enriched population of BCSCs derived from MCF7. Interestingly, cytometric analyses of SrcDN expressing mammosphere cells showed a reduction of CD44 and increased CD24 expression as compared to control mammosphere cells (non-expressing SrcDN). In addition, SrcDN induction did not induce apoptosis as PARP degradation did not occur, instead cyclin D1 expression was reduced, while Myc expression was unaltered. In this respect, we previously observed that SrcDN expression and selective c-Src tyrosine-kinase inhibitors diminish cyclin D1 expression and cell cycle progression at G1-phase in breast cancer cells [24, 43, 44]. Moreover, these mammosphere cells also showed expression of Oct3/4, Nanog pluripotency-associated transcription factors, ALDH1, and CD44 stem-cell markers [34–36], which were reduced upon SrcDN

induction. These pluripotency-associated transcription factors are required for embryonic stem cell self-renewal [34], and they are also involved in tumorigenesis and metastasis [45]. Specifically, MDA-MB-231 cells exhibit high expression of Oct3/4, and low levels of Nanog compared to MCF7 and T47D [46]. Collectively, our results suggest that c-Src functionality is essential for the self-renewal ability of BCSCs derived from MCF7 to grow in vitro as mammospheres.

MCF7 cells have been used as a model for Luminal A type of hormonal-dependent breast tumors, they have epithelial characteristics, they express E-cadherin, and are low or non-metastatic [5]. Here, we showed that mammosphere-forming cells derived from MCF7, which represented about 1.6% of total cell population, maintained their epithelial phenotype as they showed E-cadherin, but not P-cadherin staining.

Quantitative proteomic analyses of untreated and Doxy-treated mammospheres identified up to 2.759 proteins; of these proteins, 101 were differentially expressed (FDR $< 5\%$), but only 19 of them showed same tendency in two independent experiments. Among those proteins, 15 showed a reduced expression upon SrcDN induction. The gene set enrichment analysis (GSEA) of the reduced proteins revealed an inhibition of the glycolytic pathway in these tumor-initiating cells. Thus, SrcDN restricts the Warburg effect in MCF7-mammospheres, as it reduced expression of Glut-1, glucose consumption, and expression and activity of HK2, PKM, LDHA, and lactate production. Since HIF-1 and Myc are known transcription factors involved in the control of HK2 and LDHA expression [39–41], we tested whether they were modulated by induction of SrcDN. While SrcDN inhibited expression of mRNA expression of HIF-1, Myc expression both at mRNA and protein levels was not altered. In human colon adenocarcinoma LS174T and in murine melanoma B16-F10 cell lines Warburg effect requires expression of both LDH A and B [47]. Interestingly, while LDH B is expressed in TNBC cells, it is undetectable in luminal A cells, such as MCF7 [48]. Since MCT-1 expression was also inhibited upon SrcDN induction in MCF7-mammospheres, lactate accumulated intracellularly. It has been recently shown that SrcDN reduced glucose catabolism required for proliferation, migration, invasion, and tumorigenesis in cancer cells [49]. c-Src phosphorylates HK1 and HK2, rate-limiting enzymes of glycolysis, and enhances their catalytic activity [20]. Moreover, c-Src also phosphorylates LDHA at Y10, increasing its activity, which correlates with metastasis progression of clinical tumor samples of breast cancer [19], while as shown here, the dominant-negative variant of c-Src, the SrcDN counteracted these effects. In contrast, the basal oxygen consumption, ATP production, ROS, catalase, and MnSOD levels were unmodified by SrcDN expression in mammospheres, indicating that under basal conditions, the mitochondrial functionality was unaltered by SrcDN expression.

These data strongly suggest that c-Src functionality is important for the self-renewal capacity in MCF7 breast cancer stem cells, linked to glucose metabolism.

Conclusions

The findings presented in our study support the role of c-Src in the self-renewal of the enriched subpopulation of MCF7 breast cancer stem cells (BCSCs). Furthermore, results showed that c-Src functionality is a requisite for BCSCs. Src regulates Warburg effect in BCSCs, which in turn somehow controls stem-cell factors mediating stem-cell renewal. Elucidating the pathways that regulate BCSC functionality is fundamental to achieve their specific targeting.

Supporting information

S1 File.
(PDF)

Acknowledgments

Authors are grateful to L. del Peso for the GSEA of proteomics, S. Alcalá, B. Sainz, S. Guerra, C. Gamallo, P. Lastres, M.C. Mena, E. Martín-Forero, and J. Pérez for their contributions and support, L. Boscá, and J. Gonzalez-Castaño for their comments, suggestions, and reagents. Jorge Martín-Pérez and David Hardisson are members of the GEICAM (Grupo Español de Investigación en Cáncer de Mama).

Author Contributions

Conceptualization: Jorge Martín-Pérez.

Data curation: Jorge Martín-Pérez.

Formal analysis: Jorge Martín-Pérez.

Funding acquisition: Miguel Ángel Fernández-Moreno, Jorge Martín-Pérez.

Investigation: Víctor Mayoral-Varo, Annarica Calcabrini, María Pilar Sánchez-Bailón, Óscar H. Martínez-Costa, Cristina González-Páramos, Sergio Ciordia, David Hardisson, Juan J. Aragón, Miguel Ángel Fernández-Moreno, Jorge Martín-Pérez.

Methodology: Víctor Mayoral-Varo, Annarica Calcabrini, María Pilar Sánchez-Bailón, Óscar H. Martínez-Costa, Cristina González-Páramos, Sergio Ciordia, David Hardisson, Juan J. Aragón, Miguel Ángel Fernández-Moreno, Jorge Martín-Pérez.

Project administration: Jorge Martín-Pérez.

Resources: Miguel Ángel Fernández-Moreno, Jorge Martín-Pérez.

Supervision: Jorge Martín-Pérez.

Validation: Jorge Martín-Pérez.

Visualization: Jorge Martín-Pérez.

Writing – original draft: Jorge Martín-Pérez.

Writing – review & editing: Víctor Mayoral-Varo, Annarica Calcabrini, María Pilar Sánchez-Bailón, Óscar H. Martínez-Costa, Sergio Ciordia, Juan J. Aragón, Miguel Ángel Fernández-Moreno, Jorge Martín-Pérez.

References

1. Shackleton M, Vaillant F, Simpson KJ, Stingl J, Smyth GK, Asselin-Labat ML, et al. Generation of a functional mammary gland from a single stem cell. Nature. 2006; 439(7072):84–8. https://doi.org/10.1038/nature04372 PMID: 16397499.
2. Stingl J, Eirew P, Ricketson I, Shackleton M, Vaillant F, Choi D, et al. Purification and unique properties of mammary epithelial stem cells. Nature. 2006; 439(7079):993–7. https://doi.org/10.1038/nature04496 PMID: 16395311.
3. Al-Hajj M, Wicha MS, Benito-Hernandez A, Morrison SJ, Clarke MF. Prospective identification of tumorigenic breast cancer cells. Proc Natl Acad Sci U S A. 2003; 100(7):3983–8. https://doi.org/10.1073/pnas.0530291100 PMID: 12629218.
4. Marotta LL, Polyak K. Cancer stem cells: a model in the making. Curr Opin Genet Dev. 2009; 19(1):44–50. https://doi.org/10.1016/j.gde.2008.12.003 PMID: 19167210.
5. Holliday DL, Speirs V. Choosing the right cell line for breast cancer research. Breast Cancer Res. 2011; 13(4):215. Epub 2011/09/03. https://doi.org/10.1186/bcr2889 PMID: 21884641; PubMed Central PMCID: PMC3236329.
6. Thomas SM, Brugge JS. Cellular functions regulated by Src family kinases. Ann Rev Cell Dev Biol. 1997; 13:513–609.

7. Guarino M. Src signaling in cancer invasion. J Cell Physiol. 2010; 223(1):14–26. Epub 2010/01/06. https://doi.org/10.1002/jcp.22011 PMID: 20049846.

8. Espada J, Martin-Perez J. An Update on Src Family of Nonreceptor Tyrosine Kinases Biology. Int Rev Cell Mol Biol. 2017; 331:83–122. https://doi.org/10.1016/bs.ircmb.2016.09.009 PMID: 28325216.

9. Johnson FM, Gallick GE. SRC family nonreceptor tyrosine kinases as molecular targets for cancer therapy. Anticancer Agents Med Chem. 2007; 7(6):651–9. Epub 2007/11/30. https://doi.org/10.2174/187152007784111278 PMID: 18045060.

10. Wheeler DL, Iida M, Dunn EF. The role of Src in solid tumors. Oncologist. 2009; 14(7):667–78. Epub 2009/07/08. theoncologist.2009-0009 [pii] https://doi.org/10.1634/theoncologist.2009-0009 PMID: 19581523.

11. Guy CT, Muthuswamy SK, Cardiff RD, Soriano P, Muller WJ. Activation of the c-Src tyrosine kinase is required for the induction of mammary tumors in transgenic mice. Genes Dev. 1994; 8(1):23–32. https://doi.org/10.1101/gad.8.1.23 PMID: 7507074

12. Verbeek BS, Vroom TM, Adriaansen-Slot SS, Ottenhoff-Kalff AE, Geertzema JG, Hennipman A, et al. c-Src protein expression is increased in human breast cancer. An immunohistochemical and biochemical analysis. J Pathol. 1996; 180(4):383–8. https://doi.org/10.1002/(SICI)1096-9896(199612)180:4<383::AID-PATH686>3.0.CO;2-N PMID: 9014858

13. Finn RS. Targeting Src in breast cancer. Ann Oncol. 2008; 19(8):1379–86. Epub 2008/05/20. https://doi.org/10.1093/annonc/mdn291 PMID: 18487549.

14. Zhang XH, Wang Q, Gerald W, Hudis CA, Norton L, Smid M, et al. Latent bone metastasis in breast cancer tied to SRC-dependent survival signals. Cancer Cell. 2009; 16(1):67–78. Epub 2009/07/04. https://doi.org/10.1016/j.ccr.2009.05.017 PMID: 19573813.

15. Zhang S, Huang WC, Zhang L, Zhang C, Lowery FJ, Ding Z, et al. SRC family kinases as novel therapeutic targets to treat breast cancer brain metastases. Cancer Res. 2013; 73(18):5764–74. https://doi.org/10.1158/0008-5472.CAN-12-1803 PMID: 23913825; PubMed Central PMCID: PMC3781592.

16. Hoshino A, Costa-Silva B, Shen TL, Rodrigues G, Hashimoto A, Tesic Mark M, et al. Tumour exosome integrins determine organotropic metastasis. Nature. 2015; 527(7578):329–35. https://doi.org/10.1038/nature15756 PMID: 26524530.

17. DeNicola GM, Cantley LC. Cancer's Fuel Choice: New Flavors for a Picky Eater. Mol Cell. 2015; 60(4):514–23. Epub 2015/11/23. https://doi.org/10.1016/j.molcel.2015.10.018 PMID: 26590711; PubMed Central PMCID: PMC4676726.

18. Liang J, Cao R, Zhang Y, Xia Y, Zheng Y, Li X, et al. PKM2 dephosphorylation by Cdc25A promotes the Warburg effect and tumorigenesis. Nat Commun. 2016; 7:12431. https://doi.org/10.1038/ncomms12431 PMID: 27485204; PubMed Central PMCID: PMC4976202.

19. Jin L, Chun J, Pan C, Alesi GN, Li D, Magliocca KR, et al. Phosphorylation-mediated activation of LDHA promotes cancer cell invasion and tumour metastasis. Oncogene. 2017; 36(27):3797–806. https://doi.org/10.1038/onc.2017.6 PMID: 28218905; PubMed Central PMCID: PMC5501759.

20. Zhang J, Wang S, Jiang B, Huang L, Ji Z, Li X, et al. c-Src phosphorylation and activation of hexokinase promotes tumorigenesis and metastasis. Nat Commun. 2017; 8:13732. https://doi.org/10.1038/ncomms13732 PMID: 28054552; PubMed Central PMCID: PMC5227066.

21. Koppenol WH, Bounds PL, Dang CV. Otto Warburg's contributions to current concepts of cancer metabolism. Nat Rev Cancer. 2011; 11(5):325–37. Epub 2011/04/22. https://doi.org/10.1038/nrc3038 PMID: 21508971.

22. Cooper JA, Reiss NA, Schwartz RJ, Hunter T. Three glycolytic enzymes are phosphorylated at tyrosine in cells transformed by Rous sarcoma virus. Nature. 1983; 302(5905):218–23. https://doi.org/10.1038/302218a0 PMID: 6188054

23. Flier JS, Mueckler MM, Usher P, Lodish HF. Elevated levels of glucose transport and transporter messenger RNA are induced by ras or src oncogenes. Science. 1987; 235(4795):1492–5. https://doi.org/10.1126/science.3103217 PMID: 3103217.

24. Gonzalez L, Agullo-Ortuno MT, Garcia-Martinez JM, Calcabrini A, Gamallo C, Palacios J, et al. Role of c-Src in Human MCF7 Breast Cancer Cell Tumorigenesis. J Biol Chem. 2006; 281(30):20851–64. https://doi.org/10.1074/jbc.M601570200 PMID: 16728403

25. Ponti D, Costa A, Zaffaroni N, Pratesi G, Petrangolini G, Coradini D, et al. Isolation and in vitro propagation of tumorigenic breast cancer cells with stem/progenitor cell properties. Cancer Res. 2005; 65(13):5506–11. https://doi.org/10.1158/0008-5472.CAN-05-0626 PMID: 15994920.

26. Mayoral-Varo V, Calcabrini A, Sanchez-Bailon MP, Martin-Perez J. miR205 inhibits stem cell renewal in SUM159PT breast cancer cells. PLoS One. 2017; 12(11):e0188637. https://doi.org/10.1371/journal.pone.0188637 PMID: 29182685; PubMed Central PMCID: PMC5705145.

27. Munoz-Guerra MF, Marazuela EG, Fernandez-Contreras ME, Gamallo C. P-cadherin expression reduced in squamous cell carcinoma of the oral cavity: an indicatior of poor prognosis. Cancer. 2005; 103(5):960–9. https://doi.org/10.1002/cncr.20858 PMID: 15685613.

28. Perez-Riverol Y, Csordas A, Bai J, Bernal-Llinares M, Hewapathirana S, Kundu DJ, et al. The PRIDE database and related tools and resources in 2019: improving support for quantification data. Nucleic Acids Res. 2019; 47(D1):D442–D50. Epub 2018/11/06. https://doi.org/10.1093/nar/gky1106 PMID: 30395289; PubMed Central PMCID: PMC6323896.

29. Bergmeyer HU, Bergmeyer J, Grassl M. Methods of enzymatic analysis. Methods of enzymatic analysis / editor-in-chief, Hans Ulrich Bergmeyer; editors, Jürgen Bergmeyer and Marianne Grassl Edition: 3rd ed. 1983;III. NLM ID: 8508151 [Book].

30. Echevarria L, Clemente P, Hernandez-Sierra R, Gallardo ME, Fernandez-Moreno MA, Garesse R. Glutamyl-tRNAGln amidotransferase is essential for mammalian mitochondrial translation in vivo. Biochem J. 2014; 460(1):91–101. Epub 2014/03/04. https://doi.org/10.1042/BJ20131107 PMID: 24579914.

31. Adan C, Matsushima Y, Hernandez-Sierra R, Marco-Ferreres R, Fernandez-Moreno MA, Gonzalez-Vioque E, et al. Mitochondrial transcription factor B2 is essential for metabolic function in Drosophila melanogaster development. J Biol Chem. 2008; 283(18):12333–42. Epub 2008/03/01. https://doi.org/10.1074/jbc.M801342200 PMID: 18308726; PubMed Central PMCID: PMC2431005.

32. Cobb BS, Schaller MD, Leu TH, Parsons JT. Stable association of pp60src and pp59fyn with the focal adhesion-associated protein tyrosine kinase, pp125FAK. Mol Cell Biol. 1994; 14(1):147–55. https://doi.org/10.1128/mcb.14.1.147 PMID: 7505391

33. Schaller MD, Hildebrand JD, Shannon JD, Fox JW, Vines RR, Parsons JT. Autophosphorylation of the focal adhesion kinase, pp125FAK, directs SH2- dependent binding of pp60src. Mol Cell Biol. 1994; 14(3):1680–8. https://doi.org/10.1128/mcb.14.3.1680 PMID: 7509446

34. Boyer LA, Lee TI, Cole MF, Johnstone SE, Levine SS, Zucker JP, et al. Core transcriptional regulatory circuitry in human embryonic stem cells. Cell. 2005; 122(6):947–56. https://doi.org/10.1016/j.cell.2005.08.020 PMID: 16153702; PubMed Central PMCID: PMC3006442.

35. Ginestier C, Hur MH, Charafe-Jauffret E, Monville F, Dutcher J, Brown M, et al. ALDH1 Is a Marker of Normal and Malignant Human Mammary Stem Cells and a Predictor of Poor Clinical Outcome. Cell Stem Cell. 2007; 1(5):555–67. Epub 2008/03/29. https://doi.org/10.1016/j.stem.2007.08.014 PMID: 18371393.

36. Crabtree JS, Miele L. Breast Cancer Stem Cells. Biomedicines. 2018; 6(3):77. Epub 2018/07/19. https://doi.org/10.3390/biomedicines6030077 PMID: 30018256; PubMed Central PMCID: PMC6163894.

37. Oh S, Kim H, Nam K, Shin I. Glut1 promotes cell proliferation, migration and invasion by regulating epidermal growth factor receptor and integrin signaling in triple-negative breast cancer cells. BMB Rep. 2017; 50(3):132–7. https://doi.org/10.5483/bmbrep.2017.50.3.189 PMID: 27931517; PubMed Central PMCID: PMC5422025.

38. Garcia-Martinez JM, Calcabrini A, Gonzalez L, Martin-Forero E, Agullo-Ortuno MT, Simon V, et al. A non-catalytic function of the Src family tyrosine kinases controls prolactin-induced Jak2 signaling. Cell Signal. 2010; 22(3):415–26. Epub 2009/11/07. S0898-6568(09)00330-1 [pii] https://doi.org/10.1016/j.cellsig.2009.10.013 PMID: 19892015.

39. Aleshin A, Finn RS. SRC: a century of science brought to the clinic. Neoplasia. 2010; 12(8):599–607. https://doi.org/10.1593/neo.10328 PMID: 20689754; PubMed Central PMCID: PMC2915404.

40. Augoff K, Hryniewicz-Jankowska A, Tabola R. Lactate dehydrogenase 5: an old friend and a new hope in the war on cancer. Cancer Lett. 2015; 358(1):1–7. Epub 2014/12/22. https://doi.org/10.1016/j.canlet.2014.12.035 PMID: 25528630.

41. Jia D, Lu M, Jung KH, Park JH, Yu L, Onuchic JN, et al. Elucidating cancer metabolic plasticity by coupling gene regulation with metabolic pathways. Proc Natl Acad Sci U S A. 2019; 116(9):3909–18. Epub 2019/02/09. https://doi.org/10.1073/pnas.1816391116 PMID: 30733294; PubMed Central PMCID: PMC6397570.

42. Hong CS, Graham NA, Gu W, Espindola Camacho C, Mah V, Maresh EL, et al. MCT1 Modulates Cancer Cell Pyruvate Export and Growth of Tumors that Co-express MCT1 and MCT4. Cell Rep. 2016; 14(7):1590–601. Epub 2016/02/16. https://doi.org/10.1016/j.celrep.2016.01.057 PMID: 26876179; PubMed Central PMCID: PMC4816454.

43. Acosta JJ, Munoz RM, Gonzalez L, Subtil-Rodriguez A, Dominguez-Caceres MA, Garcia-Martinez JM, et al. Src mediates PRL-dependent proliferation of T47D and MCF7 cells via the activation of Fak/Erk1/2 and PI3K pathways. Mol Endocrinol. 2003; 17(11):2268–82. https://doi.org/10.1210/me.2002-0422 PMID: 12907754.

44. Sanchez-Bailon MP, Calcabrini A, Gomez-Dominguez D, Morte B, Martin-Forero E, Gomez-Lopez G, et al. Src kinases catalytic activity regulates proliferation, migration and invasiveness of MDA-MB-231

breast cancer cells. Cell Signal. 2012; 24(6):1276–86. Epub 2012/05/10. https://doi.org/10.1016/j.cellsig.2012.02.011 PMID: 22570868; PubMed Central PMCID: PMCPMID: 22570868.

45. Ben-Porath I, Thomson MW, Carey VJ, Ge R, Bell GW, Regev A, et al. An embryonic stem cell-like gene expression signature in poorly differentiated aggressive human tumors. Nat Genet. 2008; 40 (5):499–507. Epub 2008/04/30. ng.127 [pii] https://doi.org/10.1038/ng.127 PMID: 18443585.

46. Ling GQ, Chen DB, Wang BQ, Zhang LS. Expression of the pluripotency markers Oct3/4, Nanog and Sox2 in human breast cancer cell lines. Oncol Lett. 2012; 4(6):1264–8. https://doi.org/10.3892/ol.2012.916 PMID: 23197999; PubMed Central PMCID: PMC3506717.

47. Zdralevic M, Vucetic M, Daher B, Marchiq I, Parks SK, Pouyssegur J. Disrupting the 'Warburg effect' re-routes cancer cells to OXPHOS offering a vulnerability point via 'ferroptosis'-induced cell death. Adv Biol Regul. 2018; 68:55–63. Epub 2018/01/08. https://doi.org/10.1016/j.jbior.2017.12.002 PMID: 29306548.

48. McCleland ML, Adler AS, Shang Y, Hunsaker T, Truong T, Peterson D, et al. An integrated genomic screen identifies LDHB as an essential gene for triple-negative breast cancer. Cancer Res. 2012; 72 (22):5812–23. Epub 2012/11/10. https://doi.org/10.1158/0008-5472.CAN-12-1098 PMID: 23139210.

49. Lincet H, Icard P. How do glycolytic enzymes favour cancer cell proliferation by nonmetabolic functions? Oncogene. 2015; 34(29):3751–9. https://doi.org/10.1038/onc.2014.320 PMID: 25263450.

c-Src functionality controls self-renewal, tumorigenicity and glucose metabolism in breast cancer stem cells

Víctor Mayoral-Varo[1*], Annarica Calcabrini[1,2*], María Pilar Sánchez-Bailón[1,3*], Óscar H. Martínez-Costa[1], Cristina González-Páramos[1], Sergio Ciordia[4], David Hardisson[5,6], Juan J. Aragón[1], Miguel Ángel Fernández-Moreno[1,7], and Jorge Martín-Pérez[1,6,‡]

Supplementary Materials:

1. Supplementary Methods: 1.1. Gene Set Enrichment Analyses (GSEA); 1.2. RNA preparation, qRT-PCR of c-Myc and HIF-1; 1.3. Detection of mitochondrial superoxide and reactive oxygen species (ROS).

2. Supplementary figures and tables: 2.1. Figure S1. Flow cytometric analysis of isotypic immunoglobulin labeling. **2.2. Figure S2.** Three generations of mammospheres derived from MCF7-Tet-On-SrcDN. **2.3. Figure S3.** Flow cytometric analysis of CD24-PE and CD44-APC markers in control and Doxy-treated (2 μg/ml) 3rd generation mammospheres. **2.4. Figure S4.** Quantitative proteomic data from $CD24^-$ derived from MCF7-Tet-On-SrcDN. **2.5. Figure S5**. Gene set enrichment analysis (GSEA) of mammospheres derived from MCF7-Tet-On-c-SrcDN cells. **2.6. Figure S6**. c-Myc and HIF-1 expression. **2.7. Figure S7**. Profiles of oxygen consumption rates of mammospheres cells derived from MCF7-Tet-On-SrcDN. **2.8. Figure S8.** Detection of MitoSOX and ROS in $CD24^-$ cells derived from MCF7-Tet-On-SrcDN. **2.9.** List of Abbreviations. **2.10. Table S1.** Summary of quantitated proteomic analyses. **2.11. Table S2.** Antibodies employed in these studies. **2.12.** Reports of MCF7 cell line authentication. **2.13.** Figures S9, S10, S11, and S12. Uncropped scan of the western blots of the manuscript. **2.14.** Quantitation of WB.

3. References

Supplementary Materials:

1. Supplementary Methods

1.1. Gene Set Enrichment Analyses (GSEA)

The results of the quantitative proteomics analysis of BCSCs derived from MCF7-Tet-On-c-SrcDN showed a series of proteins whose levels were altered by the expression of c-SrcDN. These proteins were analyzed by GSEA, a computational method that determines whether a set of proteins/genes presents statistically significant differences between two samples.

1.2.RNA preparation, qRT-PCR of c-Myc and Hif-1

RNA was isolated from three independent experiments performed in triplicate using RNeasy kit (Qiagen). After testing for RNA integrity, triplicate RNAs from each experiment were pooled, then 1 μg of the purified RNAs was employed to synthesize the corresponding cDNAs using the Maxima First Strand cDNA Synthesis Kit for RT-qPCR with dsDNase (Thermo Fisher Scientific), followed by SYBR green (PowerUp™ SYBR™ Green Master Mix, Thermo Fisher Scientific)

RTqPCR using an Applied Biosystems StepOnePlus™ real-time thermocycler (Thermo Fisher Scientific). Cycle thresholds were normalized to β-actin levels. Expression of c-Myc and HIF-1 was determined using the following primers: c-Myc, forward 5'-CCCGCTTCTCTGAAAGGCTC TC-3', reverse 5'-CTCTGCTGCTGCTGCTGGTAG-3'; HIF-1, forward: 5'-TTGATGGGATATG AGCCAGA-3', reverse: 5'-TGTCCTGTGGTGACTTGTCC-3'; β-actin (employed to normalize), forward 5´-GCGAGCACAGAGCCTCGCCTT-3', reverse 5´-CATCATCCATGGTGAGCTGGCG G-3'. Relative expression of c-Myc and HIF-1 was calculated as the difference in cycle threshold (ΔCt) between target gene and β-actin respectively; ΔΔCt was the difference between ΔCt values of test sample and that of control. Relative expression of target genes was calculated as $2^{-\Delta\Delta Ct}$.

1.3. Detection of mitochondrial superoxide and reactive oxygen species (ROS)

Determination of Mitochondrial superoxide and ROS in CD24-neg cells derived from MCF7-Tet-ON-SrcDN in absence or presence of Doxy (2 μg/mL) was carried out employing fluorescence dies, MitoSOX red (Invitrogen, M36008), and DCFH-DA (abcam, ab113851), as described [1]. In parallel, from a portion of the same samples, the expression levels of catalase, and manganese superoxide dismutase (MnSOD) were determined by immunoblotting.

2. Supplementary figures and tables

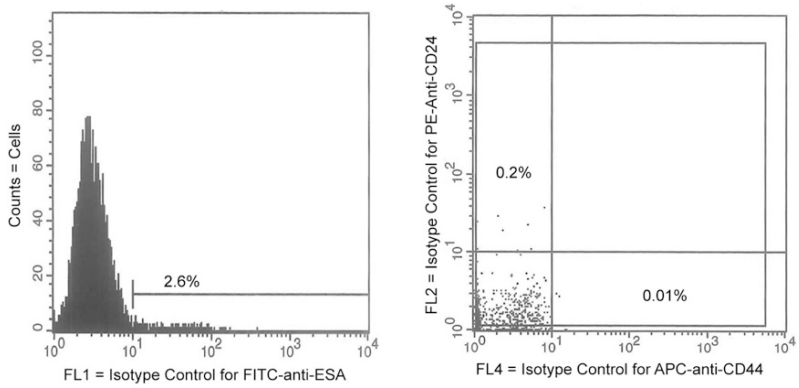

2.1. Figure S1. Flow cytometric analysis of isotypic immunoglobulin labelling. Cells were incubated with FITC-mouse IgG1 (isotypic control for ESA staining, histogram on the left), with PE-mouse IgG2a (isotypic control for CD24 labelling) and APC-mouse IgG2b (isotypic control for CD44 labelling), dot plot on the right. The percentage of positive cells are indicated. Results from one representative experiment.

Three generations of Mammospheres from MCF7-Tet-On-SrcDN

	1st generation		2nd generation		3rd generation	
	- Doxy	+ Doxy	- Doxy	+ Doxy	- Doxy	+ Doxy
Exp. 1	7.76	2.84	9.99	5.16	10.40	6.70
Exp. 2	4.99	3.44	7.95	5.43	10.80	8.80
Exp. 3	5.73	3.73	6.50	4.20	10.30	8.10
Exp. 4	8.56	4.87	8.25	6.44	9.60	3.50
Exp. 5	6.60	4.00	10.50	7.00	8.20	3.90
Mean	6.73	3.78	8.64	5.65	9.86	6.21
SD	1.5	1.0	1.6	1.0	1.0	2.0
t-Student		0.004		0.009		0.014
		p<0.01 **		p<0.01 **		p<0.5 *

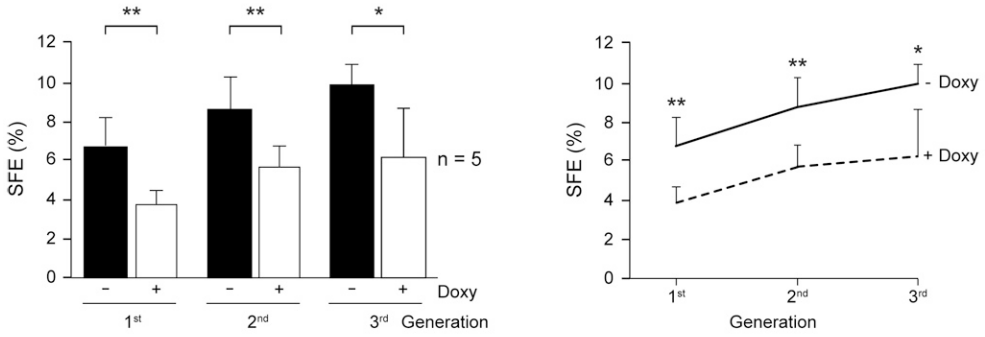

Figure S2

2.2. Figure S2. Three generations of mammospheres derived from MCF7-Tet-On-SrcDN. Cells were initially plated in 6-well ultralow attachment plates at $2x10^3$ cells/well in mammosphere culture media without Doxy. Fifteen days later, mammospheres were dissociated into single cells

that were plated in 6-well ultralow attachment plates at $2x10^3$ cells/well in mammosphere culture media, 3 wells without Doxy (Control) and 3 wells with Doxy (2 μg/ml). These two groups were maintained during the three generations, as well as during the re-plating (see Materials and methods). All experiments were carried out in triplicates. Values represent the Mean+/-SD, n=5.

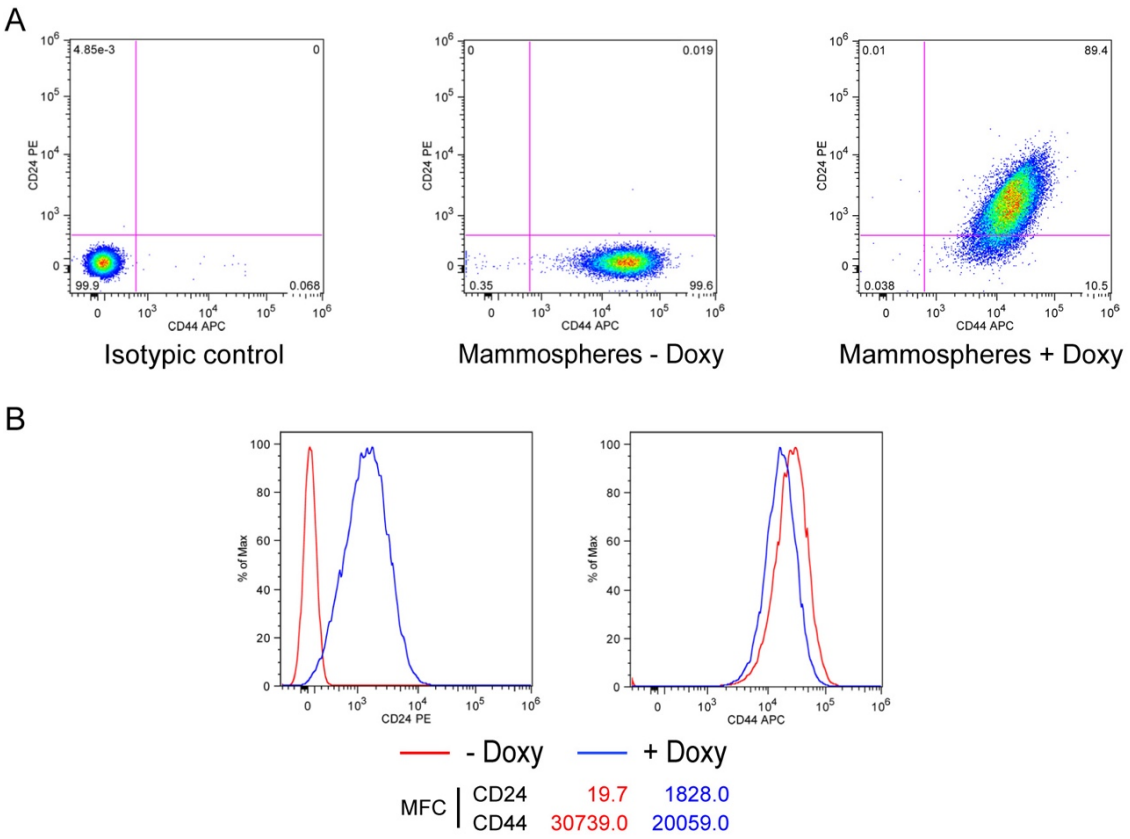

FIGURE S3. Flow cytometric analysis of CD24-PE and CD44-APC markers in control and Doxy-treated (2 μg/ml) 3rd generation mammospheres. (A) Cells obtained from dissociated mammospheres were incubated with PE-mouse IgG2a and APC-mouse IgG2b immunoglobulins (dot plot on the left, isotypic control) or with anti-CD24-PE and anti-CD44-APC monoclonal antibodies (dot plots on the right, Mammospheres -/+ Doxy). The percentage of cells in each quadrant is indicated. (B) Histograms showing CD24-PE and CD44-APC labelling in control (red line) and Doxy-treated (blue line) samples. The values of the mean fluorescence channel (MFC) related to CD24 and CD44 expression are reported. Results from one representative experiment.

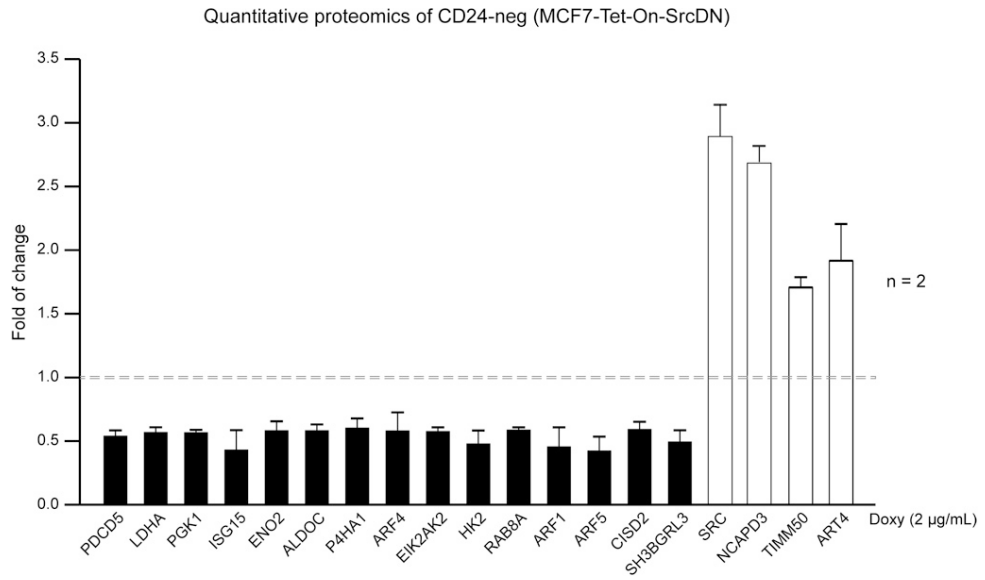

2.4. Figure S4. Quantitative proteomic data from mammospheres derived from MCF7-Tet-On-SrcDN. Graphic of bars from data shown in Table 1, refer to -Doxy considered as 1 (dashed line). Black bars showed proteins whose expression is reduced upon SrcDN induction, open bars represented proteins upregulated by SrcDN expression, showing c-Src increased up to three folds.

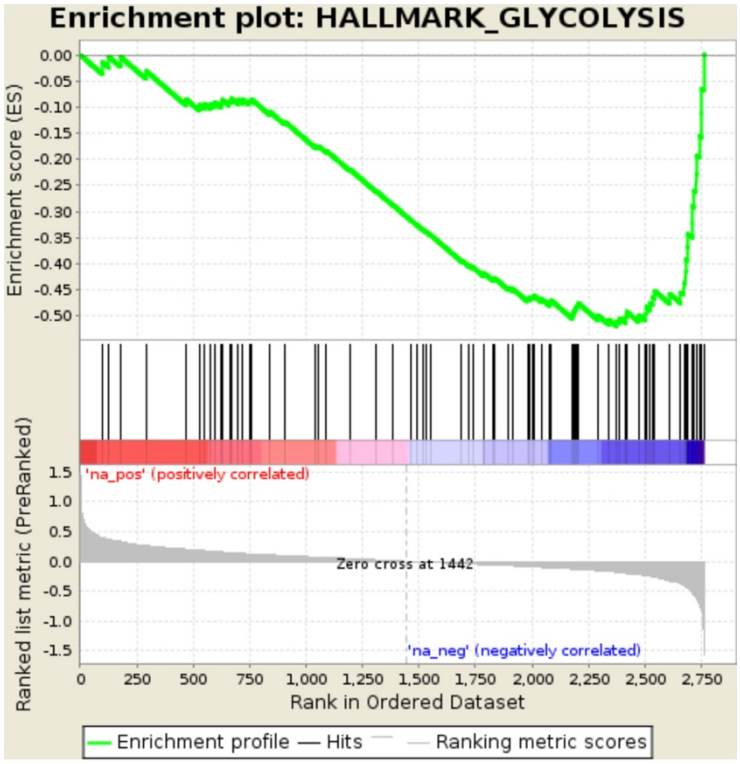

2.5. Figure S5. Gene set enrichment analysis (GSEA) of mammospheres derived from MCF7-Tet-On-c-SrcDN cells. A significant downregulation of proteins involved in glycolysis was detected in mammospheres upon expression of SrcDN.

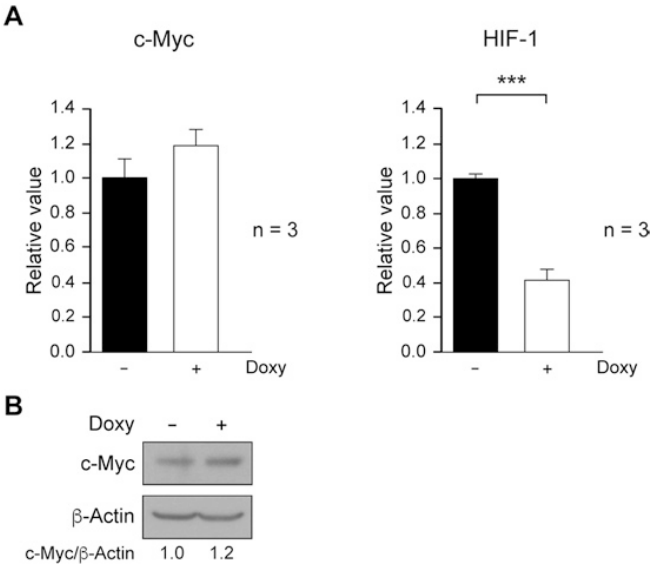

2.6. Figure S6. c-Myc and HIF-1 expression in control and Doxy-treated (2 μg/mL) 3rd mammosphere generation. (**A**) Expression of c-Myc and HIF-1 by SYBR Green q-RT-PCR using β-actin as endogenous gene (see Materials and methods). Results are shown as Mean ± SD of relative levels in three independent experiments, considering arbitrarily -Doxy (Control) as 1 (***p<0.001). (**B**) Immunoblotting analysis of c-Myc expression employing β-actin as loading control. Results are referred to -Doxy (Control) considered as 1.

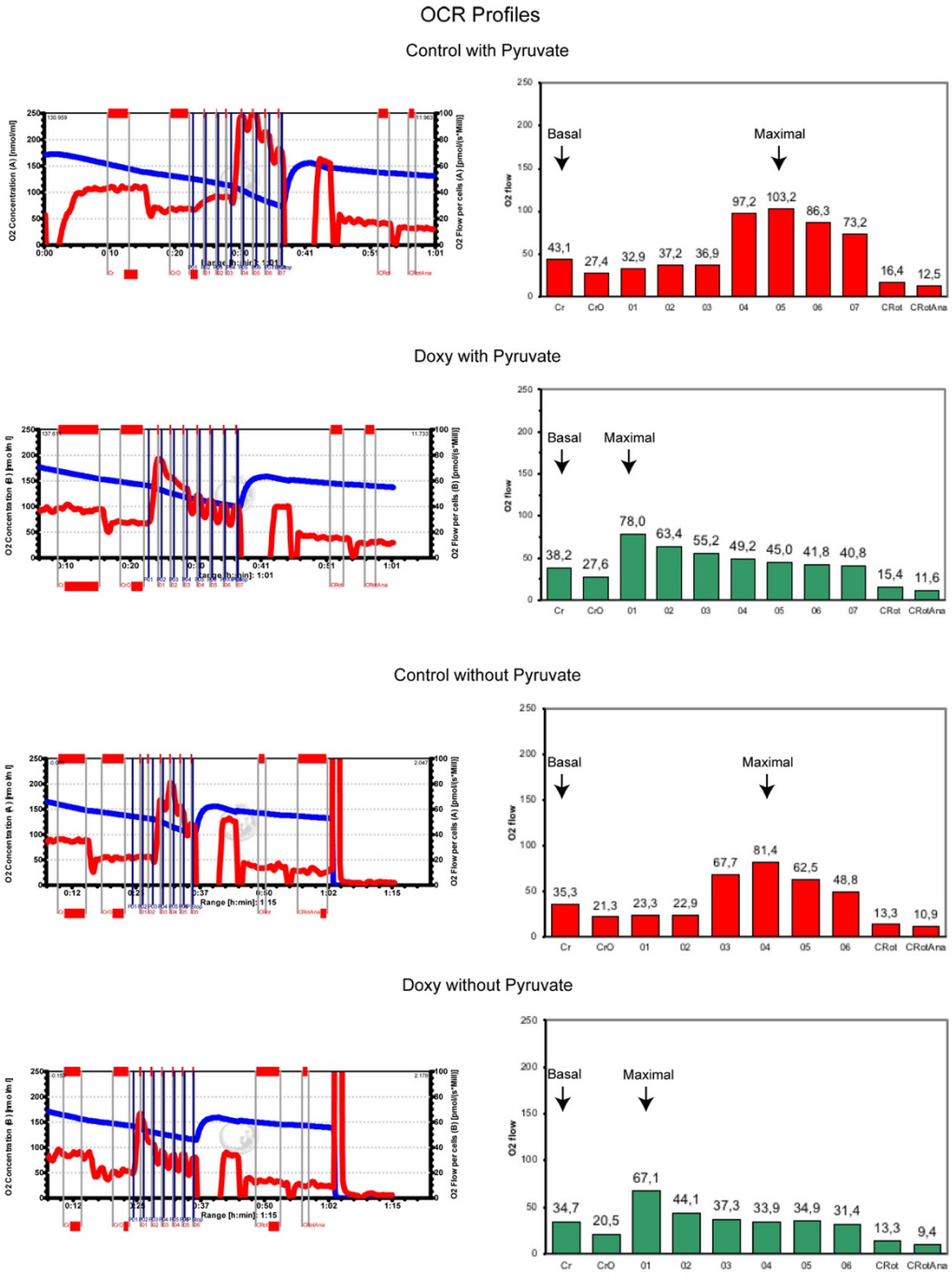

2.7. Figure S7. Profiles of oxygen consumption rates in 3rd generation mammosphere cells derived from MCF7-Tet-On-SrcDN. Experiments were carried out as described in main document. Representative profiles of OCR from mammosphere cells and graphic bars showing Basal and Maximal consumption measured in mammospheres culture media with and without pyruvate.

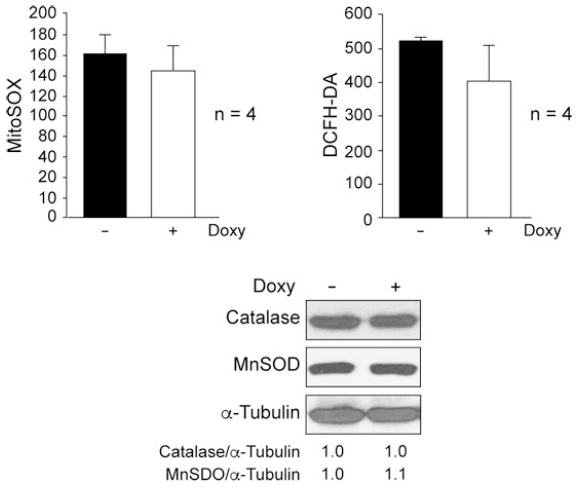

2.8. Figure S8. Detection of MitoSOX and ROS in 3rd generation mammosphere cells derived from MCF7-Tet-On-SrcDN. Mitochondrial superoxide and ROS determined in mammosphere cells derived from MCF7-Tet-ON-SrcDN in absence or presence of Doxy (2 μg/mL) was carried by flow cytometry, were quantified in arbitrary units. From a portion of the same samples, the expression levels of catalase and MnSOD from mammosphere cells was determined by immunoblotting, employing α-Tubulin as a loading control. These are representative results from 4 independent experiments. The ratios refer to -Doxy considered as 1.

c-Src functionality controls self-renewal, tumorigenicity and glucose metabolism in breast cancer stem cells, by V. Mayoral et al.

List of abbreviations:

APC	Allophycocyanin
ATP	Adenosine triphosphate
BCSCs	Breast Cancer Stem Cells
BSA	Bovine Serum Albumin
CSK	C-terminal Src Kinase
CD24-pos	CD24-high or CD24 positive
CD24-neg	CD24-low or CD24 negative
DAPI	4′, 6-diamidino-2-phenylindole
DCFH-DA	Dichloro-dihydro-fluorescein diacetate
DMEM	Dulbecco's Modified Eagle's Medium
Doxy	Doxycycline (analogue of Tetracycline)
EGF	Epidermal Growth Factor
ESA	Epithelial Specific Antigen
FCS	Fetal Calf Serum
FDR	False Discovery Rate
bFGF	basic Fibroblast Growth Factor
FITC	Fluorescein Isothiocyanate
FACS	Fluorescence-Activated Cell Sorting
Fak	Focal adhesion kinase
G6PD	Glucose-6-phosphate-Dehydrogenase
GAPDH	Glyceraldehyde-3-phosphate-Dehydrogenase
Glut-1	Glucose Transporter 1
GSEA	Gene Set Enrichment Analysis
HK	Hexokinase
LDH	Lactate dehydrogenase
MCT-1 (SLC16A1)	Proton coupled monocarboxylate transporter-1
MMP2, MMP7	Metalloproteinase 2 or 7
MnSOD	Manganese-dependent Superoxide Dismutase
MAb	Monoclonal Antibody
NAD	Nicotinamide Adenine Dinucleotide
OCR	Oxygen consumption rate
PARP	Poly (ADP-ribose) polymerases
PBS	Phosphate Buffered Saline
PE	Phycoerythrin
PK	Pyruvate Kinase
ROS	Reactive Oxygen Species
SD	Standard Deviation
SFE	Sphere Formation Efficiency (self-renewal)
SFKs	Src-family tyrosine kinases
shRNA	Short hairpin RNA
SrcDN	Dominant negative variant of c-Src (c-Src-K295M/Y527F)
Tet-On system	Doxycycline-inducible Gene Expression

From Table I

ALDOC	Fructose-bisphosphate aldolase C
ARF1	ADP-ribosylation factor 1
ARF4	ADP-ribosylation factor 4
ARF5	ADP-ribosylation factor 5
ART4	Ecto-ADP-ribosyltransferase 4
CISD2	CDSH iron-sulfur domain-containing protein
EIF2AK2	Interferon-induced, double-stranded RNA-activated protein kinase
ENO2	Gamma-enolase
HK2	Hexokinase-2
ISG15	Ubiquitin-like protein ISG15
LDHA	L-lactate dehydrogenase A chain
NCAPD3	Condensin-2 complex subunit D3
P4HA1	Prolyl 4-hydroxylase subunit alpha-1
PDCD5	Programmed cell death protein 5
PGK1	Phosphoglycerate kinase 1
RAB8A	Ras-related protein Rab-8A
SH3BGRL3	SH3 domain-binding glutamic acid-rich-like protein 3
SRC (c-Src)	Proto-oncogene tyrosine-protein kinase Src
TIMM50	Mitochondrial import inner membrane translocase subunit TIM50

2.9. List of abbreviations

DIFFERENTIAL PROTEINS FOR 5% FDR AT QUANTITATION LEVEL		Doxy-1/Control-1			Doxy-2/Control-2		
Protein_AC	Description	Ratio	Log2	FDR	Ratio	Log2	FDR
A6NFQ2	Protein FAM115C OS=Homo sapiens GN=FAM115C PE=2 SV=2	1,034	0,049	100,28%	0,660	-0,599	1,86%
O14737	Programmed cell death protein 5 OS=Homo sapiens GN=PDCD5 PE=1 SV=3	0,527	-0,923	0,33%	0,576	-0,797	0,06%
O14745	Na(+)/H(+) exchange regulatory cofactor NHE-RF1 OS=Homo sapiens GN=SLC9A3R1 PE=1 SV=4	0,845	-0,244	87,65%	0,619	-0,692	0,42%
O14773	Tripeptidyl-peptidase 1 OS=Homo sapiens GN=TPP1 PE=1 SV=2	1,235	0,304	93,56%	1,620	0,696	3,35%
O43852	Calumenin OS=Homo sapiens GN=CALU PE=1 SV=2	1,248	0,320	91,88%	0,633	-0,659	0,67%
O75506	Heat shock factor-binding protein 1 OS=Homo sapiens GN=HSBP1 PE=1 SV=1	0,504	-0,987	0,14%	0,842	-0,248	70,65%
O94855	Protein transport protein Sec24D OS=Homo sapiens GN=SEC24D PE=1 SV=2	0,906	-0,142	97,19%	0,656	-0,609	1,62%
O95197	Reticulon-3 OS=Homo sapiens GN=RTN3 PE=1 SV=2	0,593	-0,755	2,65%	0,956	-0,065	95,30%
O95400	CD2 antigen cytoplasmic tail-binding protein 2 OS=Homo sapiens GN=CD2BP2 PE=1 SV=1	1,020	0,028	99,71%	0,668	-0,581	2,43%
P00338	L-lactate dehydrogenase A chain OS=Homo sapiens GN=LDHA PE=1 SV=2	0,589	-0,764	2,36%	0,567	-0,818	0,04%
P00441	Superoxide dismutase [Cu-Zn] OS=Homo sapiens GN=SOD1 PE=1 SV=2	1,051	0,072	100,25%	0,603	-0,731	0,20%
P00558	Phosphoglycerate kinase 1 OS=Homo sapiens GN=PGK1 PE=1 SV=3	0,583	-0,777	2,05%	0,569	-0,813	0,04%
P01023	Alpha-2-macroglobulin OS=Homo sapiens GN=A2M PE=1 SV=3	0,880	-0,185	93,98%	0,457	-1,128	0,00%
P02538	Keratin, type II cytoskeletal 6A OS=Homo sapiens GN=KRT6A PE=1 SV=3	2,912	1,542	0,00%	1,101	0,139	98,08%
P02768	Serum albumin OS=Homo sapiens GN=ALB PE=1 SV=2	3,049	1,608	0,00%	1,647	0,720	2,30%
P02792	Ferritin light chain OS=Homo sapiens GN=FTL PE=1 SV=2	1,362	0,446	72,52%	0,588	-0,766	0,09%
P02794	Ferritin heavy chain OS=Homo sapiens GN=FTH1 PE=1 SV=2	0,934	-0,098	97,89%	0,630	-0,666	0,59%
P04264	Keratin, type II cytoskeletal 1 OS=Homo sapiens GN=KRT1 PE=1 SV=6	2,991	1,581	0,00%	0,927	-0,109	94,84%
P04350	Tubulin beta-4A chain OS=Homo sapiens GN=TUBB4A PE=1 SV=2	0,547	-0,871	0,68%	1,280	0,356	76,52%
P05161	Ubiquitin-like protein ISG15 OS=Homo sapiens GN=ISG15 PE=1 SV=5	0,540	-0,889	0,54%	0,337	-1,568	0,00%
P05387	60S acidic ribosomal protein P2 OS=Homo sapiens GN=RPLP2 PE=1 SV=1	0,588	-0,766	2,34%	0,809	-0,307	48,87%
P06703	Protein S100-A6 OS=Homo sapiens GN=S100A6 PE=1 SV=1	0,813	-0,298	76,92%	0,474	-1,076	0,00%
P08779	Keratin, type I cytoskeletal 16 OS=Homo sapiens GN=KRT16 PE=1 SV=4	2,164	1,114	0,13%	1,090	0,124	99,00%
P09104	Gamma-enolase OS=Homo sapiens GN=ENO2 PE=1 SV=3	0,541	-0,885	0,56%	0,642	-0,639	0,94%
P09972	Fructose-bisphosphate aldolase C OS=Homo sapiens GN=ALDOC PE=1 SV=2	0,569	-0,812	1,37%	0,612	-0,708	0,31%
P10412	Histone H1.4 OS=Homo sapiens GN=HIST1H1E PE=1 SV=2	2,303	1,204	0,03%	1,252	0,324	83,43%
P10606	Cytochrome c oxidase subunit 5B, mitochondrial OS=Homo sapiens GN=COX5B PE=1 SV=2	0,765	-0,387	62,42%	0,629	-0,669	0,59%
P10636	Microtubule-associated protein tau OS=Homo sapiens GN=MAPT PE=1 SV=5	1,072	0,100	99,29%	0,662	-0,595	1,93%
P12429	Annexin A3 OS=Homo sapiens GN=ANXA3 PE=1 SV=3	1,970	0,978	0,74%	1,353	0,437	50,49%
P12931	Proto-oncogene tyrosine-protein kinase Src OS=Homo sapiens GN=SRC PE=1 SV=3	3,079	1,622	0,00%	2,738	1,453	0,00%
P13645	Keratin, type I cytoskeletal 10 OS=Homo sapiens GN=KRT10 PE=1 SV=6	2,615	1,387	0,00%	1,497	0,582	14,78%
P13647	Keratin, type II cytoskeletal 5 OS=Homo sapiens GN=KRT5 PE=1 SV=3	3,290	1,718	0,00%	1,383	0,468	41,10%
P13674	Prolyl 4-hydroxylase subunit alpha-1 OS=Homo sapiens GN=P4HA1 PE=1 SV=2	0,572	-0,807	1,41%	0,653	-0,616	1,45%
P15559	NAD(P)H dehydrogenase [quinone] 1 OS=Homo sapiens GN=NQO1 PE=1 SV=1	1,911	0,935	1,36%	1,363	0,447	46,57%
P15941	Mucin-1 OS=Homo sapiens GN=MUC1 PE=1 SV=3	0,719	-0,477	41,20%	0,685	-0,546	4,33%
P16188	HLA class I histocompatibility antigen, A-30 alpha chain OS=Homo sapiens GN=HLA-A PE=1 SV=2	0,762	-0,392	62,05%	0,593	-0,754	0,12%
P16455	Methylated-DNA--protein-cysteine methyltransferase OS=Homo sapiens GN=MGMT PE=1 SV=1	1,006	0,009	99,80%	1,775	0,828	0,41%
P16949	Stathmin OS=Homo sapiens GN=STMN1 PE=1 SV=3	0,800	-0,322	74,31%	0,669	-0,580	2,43%
P17655	Calpain-2 catalytic subunit OS=Homo sapiens GN=CAPN2 PE=1 SV=6	2,078	1,055	0,27%	0,988	-0,018	98,23%
P18085	ADP-ribosylation factor 4 OS=Homo sapiens GN=ARF4 PE=1 SV=3	0,494	-1,017	0,09%	0,684	-0,549	4,15%
P19525	Interferon-induced, double-stranded RNA-activated protein kinase OS=Homo sapiens GN=EIF2AK2 PE=1 SV=2	0,571	-0,807	1,43%	0,594	-0,751	0,13%
P20933	N(4)-(beta-N-acetylglucosaminyl)-L-asparaginase OS=Homo sapiens GN=AGA PE=1 SV=2	2,058	1,042	0,33%	1,388	0,473	40,60%
P30838	Aldehyde dehydrogenase, dimeric NADP-preferring OS=Homo sapiens GN=ALDH3A1 PE=1 SV=3	1,980	0,986	0,68%	1,574	0,655	6,25%
P35527	Keratin, type I cytoskeletal 9 OS=Homo sapiens GN=KRT9 PE=1 SV=3	3,190	1,674	0,00%	0,696	-0,523	6,20%
P35908	Keratin, type II cytoskeletal 2 epidermal OS=Homo sapiens GN=KRT2 PE=1 SV=2	2,641	1,401	0,00%	1,557	0,639	7,66%
P40616	ADP-ribosylation factor-like protein 1 OS=Homo sapiens GN=ARL1 PE=1 SV=1	0,595	-0,750	2,83%	0,777	-0,364	35,74%
P42224	Signal transducer and activator of transcription 1-alpha/beta OS=Homo sapiens GN=STAT1 PE=1 SV=2	0,728	-0,459	45,86%	0,580	-0,785	0,07%
P42695	Condensin-2 complex subunit D3 OS=Homo sapiens GN=NCAPD3 PE=1 SV=2	2,595	1,376	0,00%	2,776	1,473	0,00%

P43487	Ran-specific GTPase-activating protein OS=Homo sapiens GN=RANBP1 PE=1 SV=1	0,836	-0,258	84,90%	**0,636**	**-0,653**	**0,74%**
P45973	Chromobox protein homolog 5 OS=Homo sapiens GN=CBX5 PE=1 SV=1	0,896	-0,158	97,12%	**0,666**	**-0,586**	**2,26%**
P49207	60S ribosomal protein L34 OS=Homo sapiens GN=RPL34 PE=1 SV=3	**1,859**	**0,894**	**2,05%**	1,163	0,218	95,08%
P51153	Ras-related protein Rab-13 OS=Homo sapiens GN=RAB13 PE=1 SV=1	0,774	-0,370	65,52%	**0,674**	**-0,570**	**2,88%**
P51858	Hepatoma-derived growth factor OS=Homo sapiens GN=HDGF PE=1 SV=1	0,821	-0,285	79,15%	**0,452**	**-1,144**	**0,00%**
P52789	Hexokinase-2 OS=Homo sapiens GN=HK2 PE=1 SV=2	**0,546**	**-0,874**	**0,67%**	**0,428**	**-1,226**	**0,00%**
P54252	Ataxin-3 OS=Homo sapiens GN=ATXN3 PE=1 SV=4	1,524	0,608	37,92%	**1,661**	**0,732**	**1,85%**
P56589	Peroxisomal biogenesis factor 3 OS=Homo sapiens GN=PEX3 PE=1 SV=1	**0,588**	**-0,765**	**2,33%**	0,870	-0,200	79,65%
P61006	Ras-related protein Rab-8A OS=Homo sapiens GN=RAB8A PE=1 SV=1	**0,585**	**-0,773**	**2,14%**	**0,606**	**-0,722**	**0,24%**
P62158	Calmodulin OS=Homo sapiens GN=CALM1 PE=1 SV=2	1,147	0,197	97,93%	**0,586**	**-0,770**	**0,09%**
P62330	ADP-ribosylation factor 6 OS=Homo sapiens GN=ARF6 PE=1 SV=2	**0,507**	**-0,979**	**0,16%**	0,773	-0,371	33,35%
P68366	Tubulin alpha-4A chain OS=Homo sapiens GN=TUBA4A PE=1 SV=1	**1,818**	**0,862**	**3,05%**	0,963	-0,054	95,41%
P80303	Nucleobindin-2 OS=Homo sapiens GN=NUCB2 PE=1 SV=2	**2,128**	**1,089**	**0,18%**	1,565	0,647	6,88%
P84077	ADP-ribosylation factor 1 OS=Homo sapiens GN=ARF1 PE=1 SV=2	**0,363**	**-1,464**	**0,00%**	**0,559**	**-0,838**	**0,03%**
P84085	ADP-ribosylation factor 5 OS=Homo sapiens GN=ARF5 PE=1 SV=2	**0,365**	**-1,452**	**0,00%**	**0,497**	**-1,009**	**0,00%**
Q01650	Large neutral amino acids transporter small subunit 1 OS=Homo sapiens GN=SLC7A5 PE=1 SV=2	**2,081**	**1,057**	**0,27%**	0,948	-0,077	95,84%
Q08380	Galectin-3-binding protein OS=Homo sapiens GN=LGALS3BP PE=1 SV=1	0,631	-0,664	7,92%	**0,402**	**-1,315**	**0,00%**
Q13185	Chromobox protein homolog 3 OS=Homo sapiens GN=CBX3 PE=1 SV=4	0,898	-0,155	97,30%	**0,681**	**-0,554**	**3,83%**
Q13268	Dehydrogenase/reductase SDR family member 2, mitochondrial OS=Homo sapiens GN=DHRS2 PE=1 SV=4	1,498	0,583	45,23%	**0,630**	**-0,667**	**0,60%**
Q14244	Ensconsin OS=Homo sapiens GN=MAP7 PE=1 SV=1	**1,864**	**0,898**	**2,02%**	1,108	0,148	97,92%
Q14683	Structural maintenance of chromosomes protein 1A OS=Homo sapiens GN=SMC1A PE=1 SV=2	**0,531**	**-0,912**	**0,39%**	0,919	-0,122	93,63%
Q14956	Transmembrane glycoprotein NMB OS=Homo sapiens GN=GPNMB PE=1 SV=2	**5,566**	**2,477**	**0,00%**	**1,765**	**0,820**	**0,45%**
Q15125	3-beta-hydroxysteroid-Delta(8),Delta(7)-isomerase OS=Homo sapiens GN=EBP PE=1 SV=3	1,571	0,651	27,03%	**0,614**	**-0,704**	**0,34%**
Q16881	Thioredoxin reductase 1, cytoplasmic OS=Homo sapiens GN=TXNRD1 PE=1 SV=3	**2,022**	**1,016**	**0,47%**	1,274	0,349	76,64%
Q3ZCQ8	Mitochondrial import inner membrane translocase subunit TIM50 OS=Homo sapiens GN=TIMM50 PE=1 SV=2	**1,769**	**0,823**	**4,91%**	**1,673**	**0,743**	**1,65%**
Q53HC9	Protein TSSC1 OS=Homo sapiens GN=TSSC1 PE=1 SV=2	**1,805**	**0,852**	**3,44%**	1,509	0,594	13,37%
Q53SF7	Cordon-bleu protein-like 1 OS=Homo sapiens GN=COBLL1 PE=1 SV=2	0,897	-0,157	97,28%	**1,758**	**0,814**	**0,50%**
Q58FF6	Putative heat shock protein HSP 90-beta 4 OS=Homo sapiens GN=HSP90AB4P PE=5 SV=1	**4,042**	**2,015**	**0,00%**	1,040	0,057	100,69%
Q5RKV6	Exosome complex component MTR3 OS=Homo sapiens GN=EXOSC6 PE=1 SV=1	1,330	0,412	76,64%	**1,769**	**0,823**	**0,43%**
Q8N5K1	CDGSH iron-sulfur domain-containing protein 2 OS=Homo sapiens GN=CISD2 PE=1 SV=1	**0,567**	**-0,818**	**1,36%**	**0,636**	**-0,652**	**0,75%**
Q8NEZ2	Vacuolar protein sorting-associated protein 37A OS=Homo sapiens GN=VPS37A PE=1 SV=1	1,265	0,340	89,30%	**0,485**	**-1,044**	**0,00%**
Q8WVY7	Ubiquitin-like domain-containing CTD phosphatase 1 OS=Homo sapiens GN=UBLCP1 PE=1 SV=2	**1,930**	**0,949**	**1,14%**	0,969	-0,046	96,18%
Q93070	Ecto-ADP-ribosyltransferase 4 OS=Homo sapiens GN=ART4 PE=2 SV=2	**2,120**	**1,084**	**0,18%**	**1,746**	**0,804**	**0,59%**
Q96GW9	Methionine--tRNA ligase, mitochondrial OS=Homo sapiens GN=MARS2 PE=1 SV=2	1,139	0,188	97,48%	**1,951**	**0,964**	**0,03%**
Q96HE7	ERO1-like protein alpha OS=Homo sapiens GN=ERO1L PE=1 SV=2	0,901	-0,151	96,74%	**0,651**	**-0,618**	**1,41%**
Q99622	Protein C10 OS=Homo sapiens GN=C12orf57 PE=1 SV=1	**0,317**	**-1,658**	**0,00%**	**0,586**	**-0,771**	**0,09%**
Q99988	Growth/differentiation factor 15 OS=Homo sapiens GN=GDF15 PE=1 SV=3	**1,862**	**0,897**	**2,03%**	1,325	0,406	63,48%
Q9BQE5	Apolipoprotein L2 OS=Homo sapiens GN=APOL2 PE=1 SV=1				**0,688**	**-0,539**	**4,83%**
Q9BU89	Deoxyhypusine hydroxylase OS=Homo sapiens GN=DOHH PE=1 SV=1	1,039	0,055	99,94%	**1,888**	**0,917**	**0,07%**
Q9GZM5	Protein YIPF3 OS=Homo sapiens GN=YIPF3 PE=1 SV=1	**1,795**	**0,844**	**3,78%**	0,854	-0,227	75,18%
Q9H299	SH3 domain-binding glutamic acid-rich-like protein 3 OS=Homo sapiens GN=SH3BGRL3 PE=1 SV=1	**0,550**	**-0,862**	**0,74%**	**0,454**	**-1,139**	**0,00%**
Q9H3K6	BolA-like protein 2 OS=Homo sapiens GN=BOLA2 PE=1 SV=1	0,891	-0,166	94,93%	**0,657**	**-0,606**	**1,69%**
Q9H4I2	Zinc fingers and homeoboxes protein 3 OS=Homo sapiens GN=ZHX3 PE=1 SV=3	0,900	-0,151	96,95%	**0,657**	**-0,605**	**1,66%**
Q9NP97	Dynein light chain roadblock-type 1 OS=Homo sapiens GN=DYNLRB1 PE=1 SV=3	0,676	-0,564	21,13%	**0,637**	**-0,650**	**0,77%**
Q9NZT2	Opioid growth factor receptor OS=Homo sapiens GN=OGFR PE=1 SV=3	**0,553**	**-0,855**	**0,79%**	0,731	-0,451	14,41%
Q9NZZ3	Charged multivesicular body protein 5 OS=Homo sapiens GN=CHMP5 PE=1 SV=1	0,978	-0,033	99,42%	**0,671**	**-0,576**	**2,61%**
Q9P2D3	HEAT repeat-containing protein 5B OS=Homo sapiens GN=HEATR5B PE=1 SV=2	**0,562**	**-0,831**	**1,12%**	0,986	-0,020	98,15%
Q9UIG0	Tyrosine-protein kinase BAZ1B OS=Homo sapiens GN=BAZ1B PE=1 SV=2	1,275	0,351	87,99%	**1,752**	**0,809**	**0,54%**
Q9UII2	ATPase inhibitor, mitochondrial OS=Homo sapiens GN=ATPIF1 PE=1 SV=1	0,756	-0,404	58,80%	**0,565**	**-0,823**	**0,03%**
Q9UK22	F-box only protein 2 OS=Homo sapiens GN=FBXO2 PE=1 SV=2	**0,568**	**-0,816**	**1,33%**	0,780	-0,358	37,06%

Q9UNL2	Translocon-associated protein subunit gamma OS=Homo sapiens GN=SSR3 PE=1 SV=1	**0,600**	**-0,737**	**3,36%**	0,966	-0,050	95,56%
Q9Y2K7	Lysine-specific demethylase 2A OS=Homo sapiens GN=KDM2A PE=1 SV=3	0,964	-0,053	99,25%	**1,686**	**0,753**	**1,41%**
Q9Y6K5	2~-5~-oligoadenylate synthase 3 OS=Homo sapiens GN=OAS3 PE=1 SV=3	**0,429**	**-1,220**	**0,00%**	0,769	-0,380	31,08%

Down-expressed
Up-expressed

Significant (FDR<1%)
Significant (1%<FDR<5%)
Non-significant FDR>5%

2.10. Table S1. Summary of quantitated proteomics analyses from MCF7-Tet-On-SrcDN mammospheres.

Table S2. Detailed information for antibodies used in this work.

Name	Type	Supplier	Catalog #	Origin	Dilution Ratio WB*-FC/IF**-IHC***
β-Actin	mouse monoclonal	Sigma-Aldrich (Merck)	A5441	San Luis, MI, USA	1:1000-….-….
ALDH1	mouse monoclonal	BD-Biosciences	#611194	Franklin Lakes, NJ, USA	1:500-….-….
Cadherin-E	mouse monoclonal	A. Cano		IIB (UAM/CSIC)	1:200_1:50_1:20
Cadherin-P (clone 56C1)	mouse monoclonal	Novocastra Laboratories	#610227	Newcastle, UK	….-….-1:200
CD44-APC	mouse monoclonal	BD-Biosciences	#559942FIT	Franklin Lakes, NJ, USA	….-1:20-….
CD24-PE	mouse monoclonal	BD-Biosciences	#555428	Franklin Lakes, NJ, USA	….-1:20-….
Catalase	mouse monoclonal	Sigma-Aldrich (Merck)	#C0979	San Luis, MI, USA	1:1000_…._….
Cyclin D1 (H-295)	rabbit polyclonal	Santa Cruz Biotechnology, Inc.	sc-753	Dallas, TX, USA	1:1000-….-….
c-Src (MAb-327)	mouse monoclonal	J.S. Brugge (Harvard University)		Harvard University, MA, USA	1:1000-….-….
c-Src (MAb EC10)	mouse monoclonal	Millipore (Merk)	#05-185	Billerica, MA, USA	1:1000-….-….
c-Src-pY418	rabbit polyclonal	Invitrogen	#44660G	Camarillo, CA, USA	1:1000-….-….
Envision-peroxidase anti-mouse polymer labeled with HRP	goat polyclonal	Dako Corporation	K4000	Carpinteria, CA, USA	…._….._1:100
ESA-FITC	mouse monoclonal	Biomeda Corp.	FM010	Foster City, CA, USA	…._…._1:20
Fak	rabbit polyclonal	Santa Cruz Biotechnology, Inc.	Sc-557	Dallas, TX, USA	1:1000-….-….
Fak-pY397	mouse monoclonal	BD-Biosciences	#611722	Franklin Lakes, NJ, USA	1:1000-….-….
GAPDH (clone 6C5)	mouse monoclonal	Millipore (Merk)	CB1001	Billerica, MA, USA	1:4000_…._….
Glut-1	rabbit polyclonal	Santa Cruz Biotechnology, Inc.	Sc-7903	Dallas, TX, USA	1:1000-….-….
HK2	rabbit polyclonal	Cell Signaling Technology	#C64G5	Danvers, MA, USA	1:1000-….-….
LDHA	rabbit polyclonal	Cell Signaling Technology	#3582	Danvers, MA, USA	1:1000-….-….
LDHA-pY10	rabbit polyclonal	cell Signaling Technology	#8176	Danvers, MA, USA	1:1000-….-….
Mn-SOD	rabbit polyclonal	Millipore (Merck)	#06-984	Billerica, MA, USA	1:1000-…._….
MCT-1	mouse monoclonal	Santa Cruz Biotechnology, Inc.	Sc-365501	Dallas, TX, USA	1:1000-….-….
Nanog	rabbit polyclonal	Millipore (Merk)	#AB9220	Billerica, MA, USA	1:1000-….-….
Oct3/4	goat polyclonal	Santa Cruz Biotechnology, Inc.	Sc-8629	Dallas, TX, USA	1:100-….-….
PARP (clone C-2-10)	mouse monoclonal	Biomol Gmbh	SA-249	Hamburg, Gemany	1:1000-….-….
α-Tubulin	mouse monoclonal	Sigma-Aldrich (Merck)	T9026	San Luis, MI, USA	1:8000-….-….

Western Blotting (WB)*
Flow-cytometry (FC)/Immunofluorescence (IF)**
Immunohistochemistry (IHC)***

2.11. Table S2. Antibodies employed in these studies.

1

HUMAN CELL LINE STR PROFILE REPORT

CELL LINE DESCRIPTION according to customer: MCF7 (ATCC ® HTB-22/CVCL_0031)

Sample Submitted By:

Jorge Martín Pérez
Instituto de Investigaciones Biomédicas. CSIC
jmartin@iib.uam.es

Date: 13.12.2018
Microsatellite Run Number (pdf attached): M192
Laboratory:

Genomics Core Facility.
Instituto de Investigaciones Biomédicas "Alberto Sols" CSIC-UAM.
28029 Madrid
00 34 91 585 44 74 (Tel.) 00 34 91 585 44 01 (Fax)
genomica@iib.uam.es

STR PROFILE DATA:

STR PROFILE OBTAINED		EXPECTED
D5S818	12	11,12
D13S317	11	11
D7S820	8,9	8,9
D16S539	11,12	11,12
vWA	14,15	14,15
TH01	6	6
TPOX	9,12	9,12
CSF1PO	10	10
D21S11	30	
Amelogenin	X	X
RESULTS		
Number of shared alleles: 15		
Number of alleles in database: 16		
Percent match: 93%		

TEST RESULTS:
Query profiles were sent against ATCC database
Cell lines with ≥80% match are considered to be related (i.e common ancestor).
Cell lines with 55%-80% match require further profiling

- ✓ The submitted sample profile is human and matches 93% with customer cell line description
- The submitted sample profile is human, but does not match customer cell line description
- No human STRs are amplified

DATABASE OUTPUT:

%Match	ATCC® Number	Designation	D5S818	D13S317	D7S820	D16S539	vWA	TH01	AMEL	TPOX	CSF1PO
93.0	HTB-22	MCF7Breast AdenocarcinomaHuman	11,12	11	8,9	11,12	14,15	6	X	9,12	10

METHOD:

STR ANALYSIS	
STR amplification kit	GenePrint® 10 System (Promega)
STR profile analysis software	GeneMapper® v3.7 (Life Technologies)
Genomic Analyzer System	ABI 3130 XL (Applied Biosystems)
DNA source	Cultured cells; cultured cells pellet
DNA isolation method	DNeasy blood and tissue kit (Qiagen)
DNA quantification method	Qubit 2.0 Fluorometer (Life Technologies)
Amount of DNA/amplification	4 ng

The *GenePrint*® 10 System allows co-amplification and three-color detection of ten human loci: TH01, TPOX, vWA, Amelogenin, CSF1PO, D16S539, D7S820, D13S317, D21S11 and D5S818. These loci collectively provide a genetic profile with a random match probability of 1 in 2.92×10^9 and are used for human cell line and tissue authentication and identification and human cell line cross-contamination determination. Samples are processed using the ABI Prism® 31300xl Genetic Analyzer. Data are analyzed using GeneMapper® ID-X v1.2 software (Applied Biosystems). STRs profiles are sent for comparison against cell line date bases like ATCC (American Type Culture Collection), DSMZ (Deutsche Sammlung von Mikrorganismen and Zellkulturen)...

2

HUMAN CELL LINE STR PROFILE REPORT

ELECTROPHEROGRAM

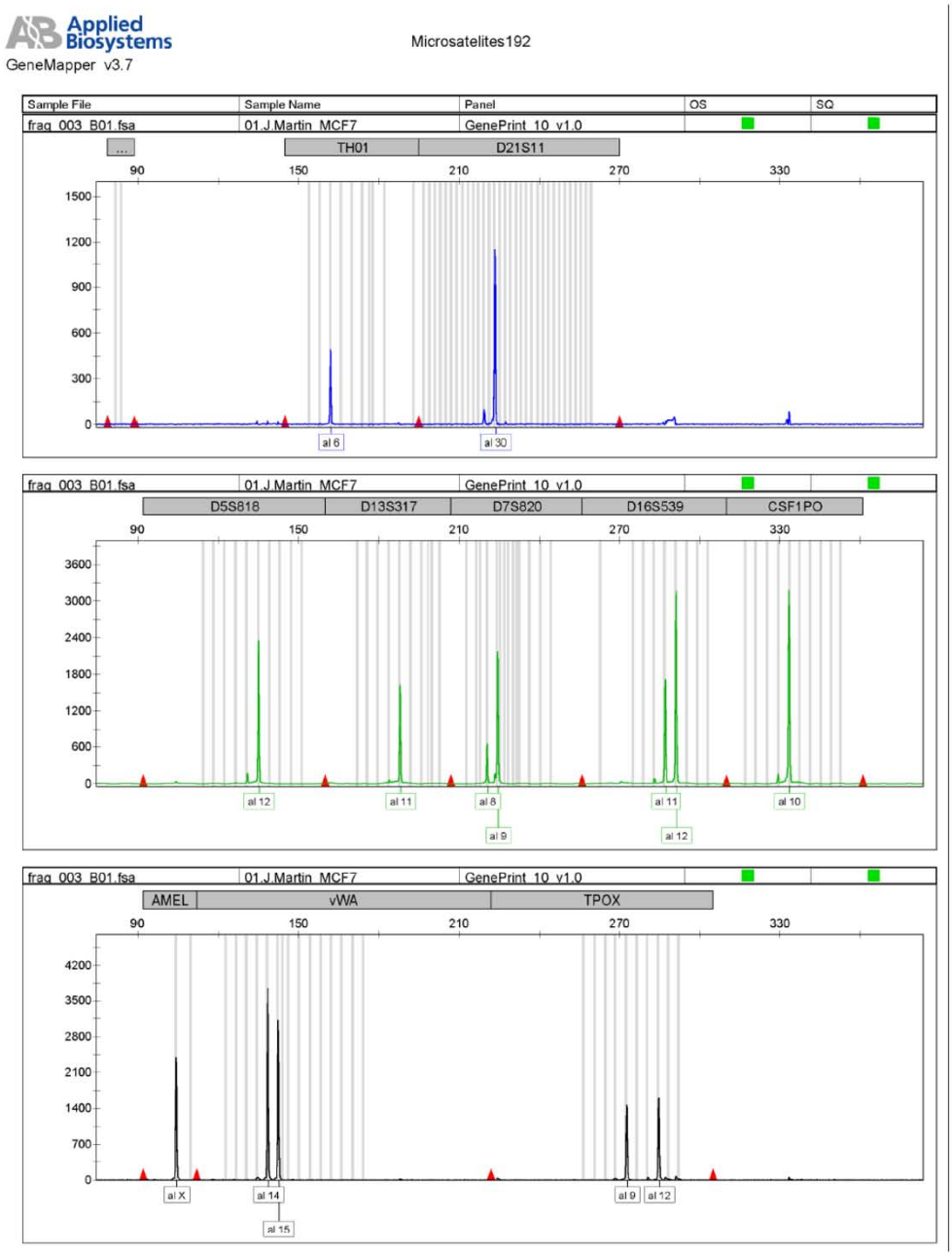

2.12. Reports of MCF7 cell line authentication. MCF7 cell line was authenticated by short-tandem-repeat analysis (GenePrintR 10 System from Promega, and GeneMapper v3.7 STR profile analysis software, Life Technologies).

Uncropped Immunoblots from Figure_1

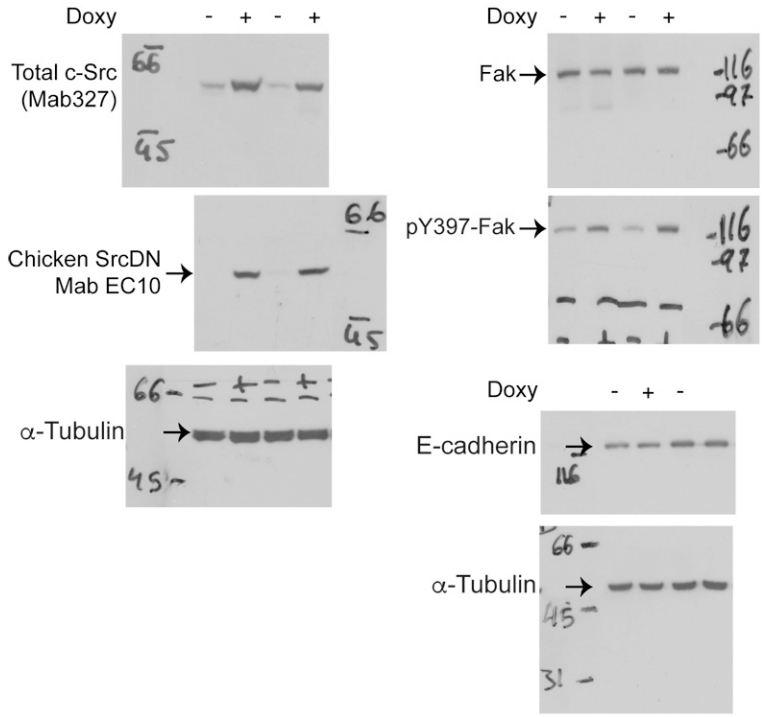

9

Uncropped Immunoblots from Figure_2

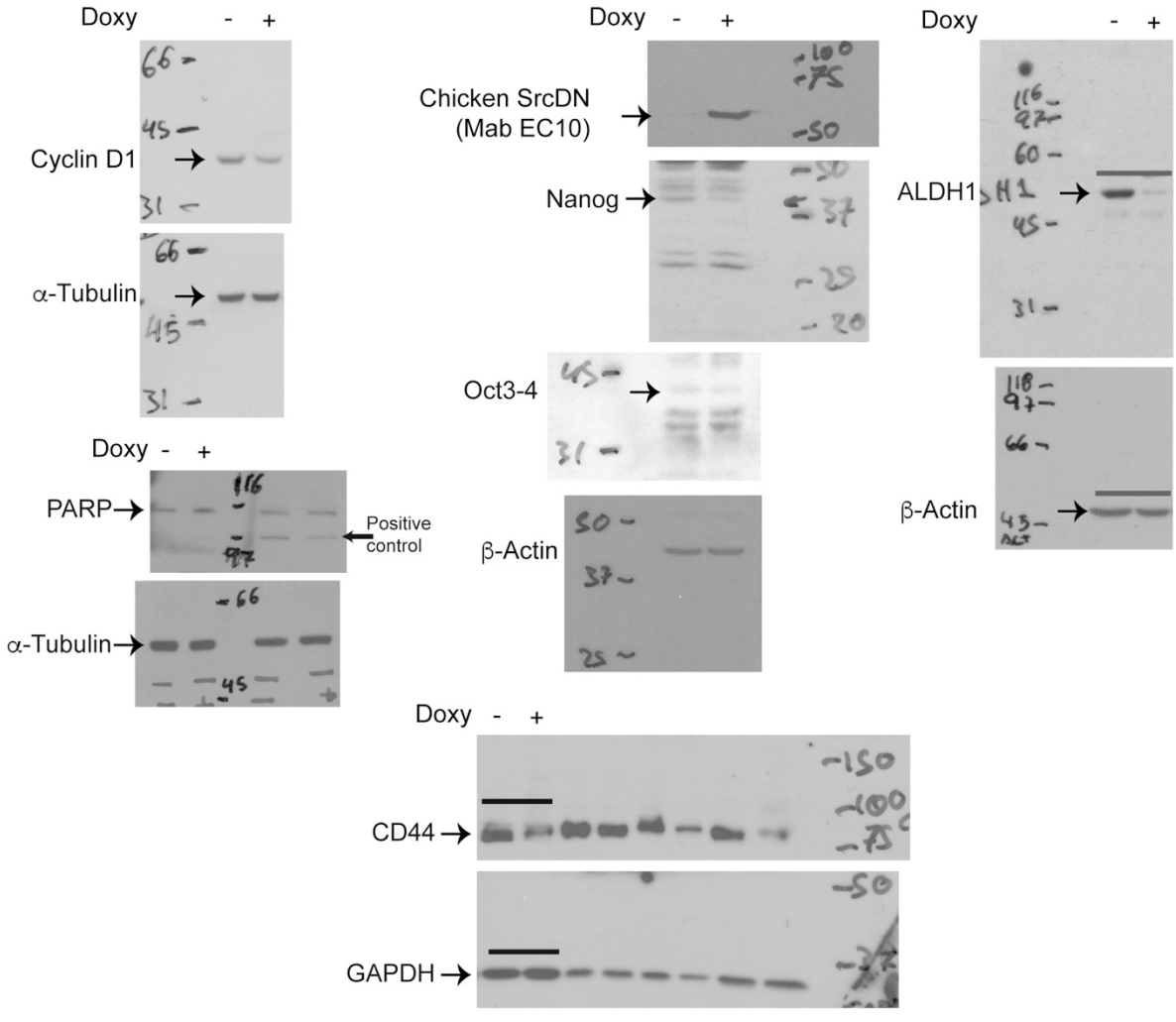

10

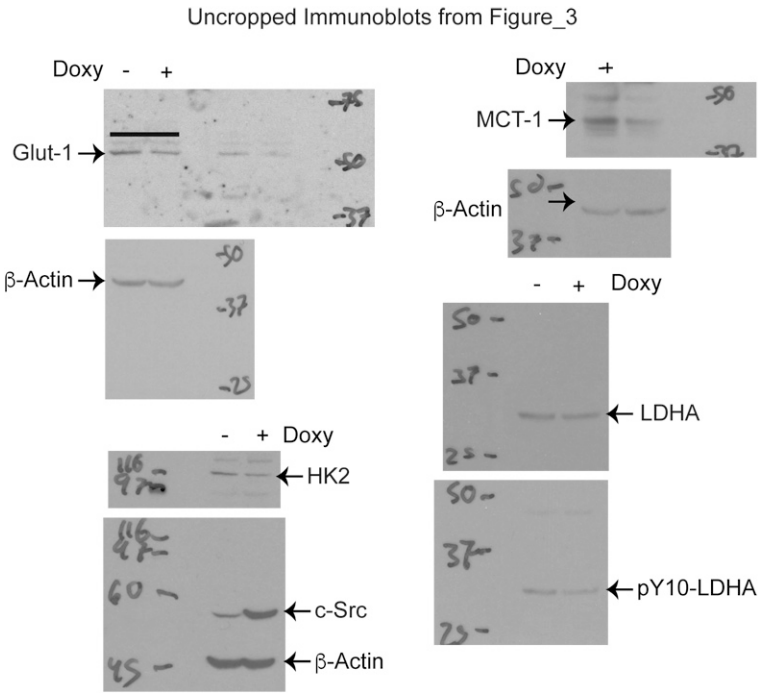

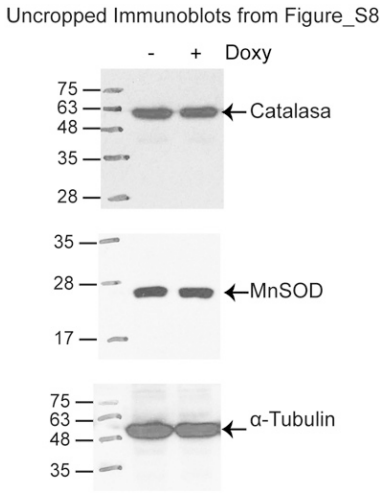

2.13. Figure. Uncropped scan of the western blots of the manuscript. Since it was difficult (time consuming) to obtain large amounts of samples, we cut the transfer membranes to incubate each of them with antibodies to obtain different results from a single immunoblotting membrane.

MCF7-Tet-On-SrcDN_Mammospheres (FIGURE 1)

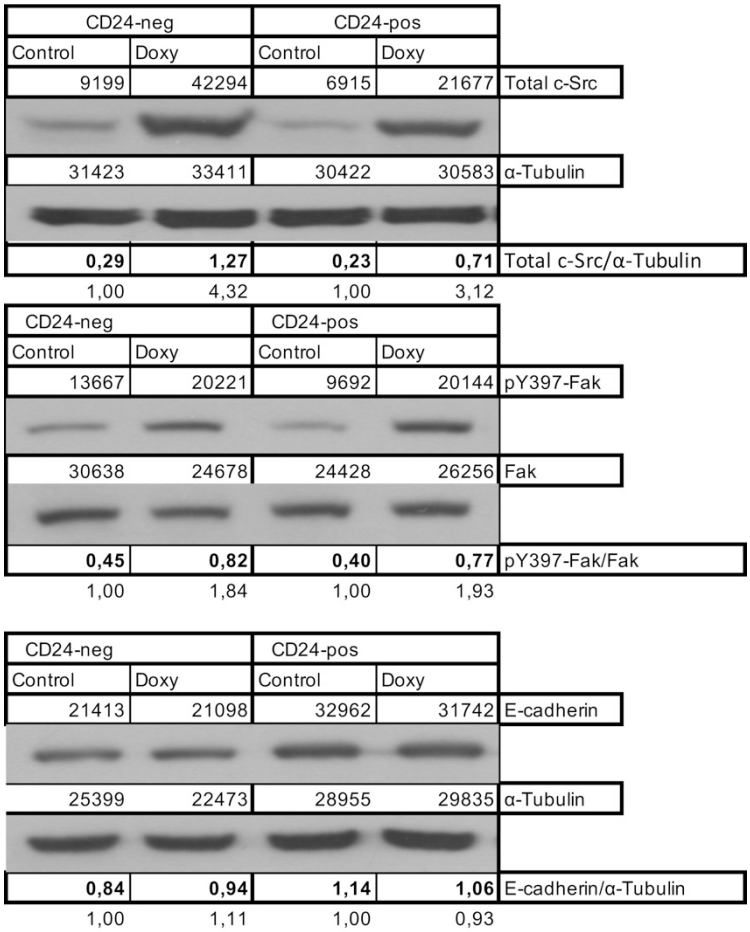

18

MCF7-Tet-On-SrcDN Mammospheres (FIGURE 2)

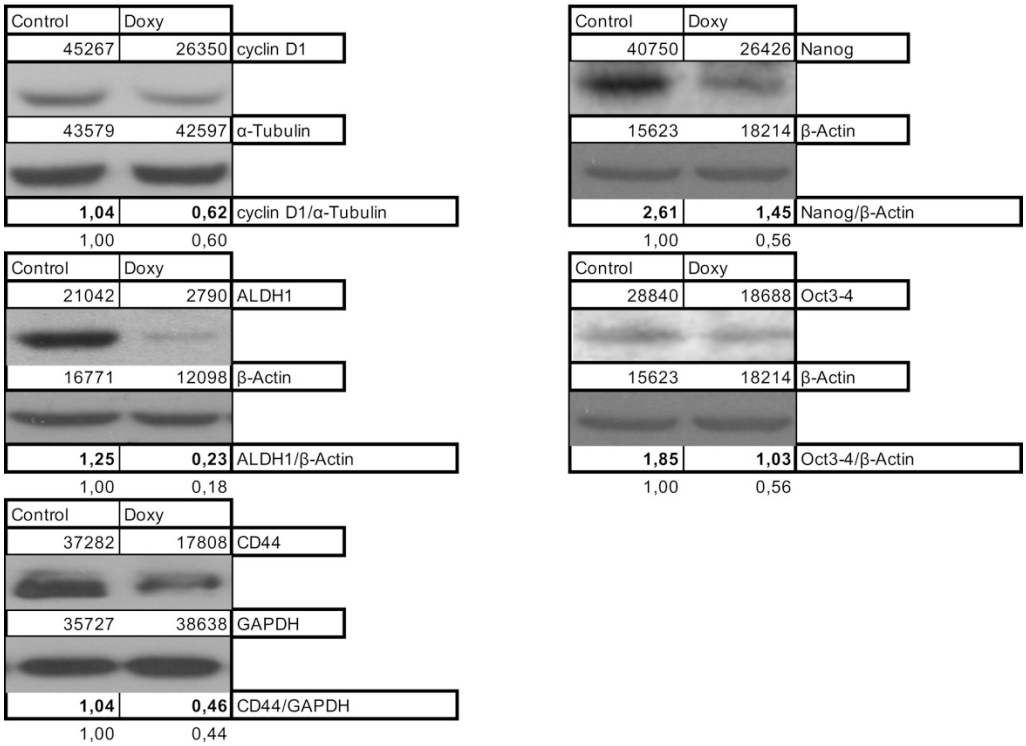

19

MCF7-Tet-On-SrcDN_Mammospheres (FIGURE 3)

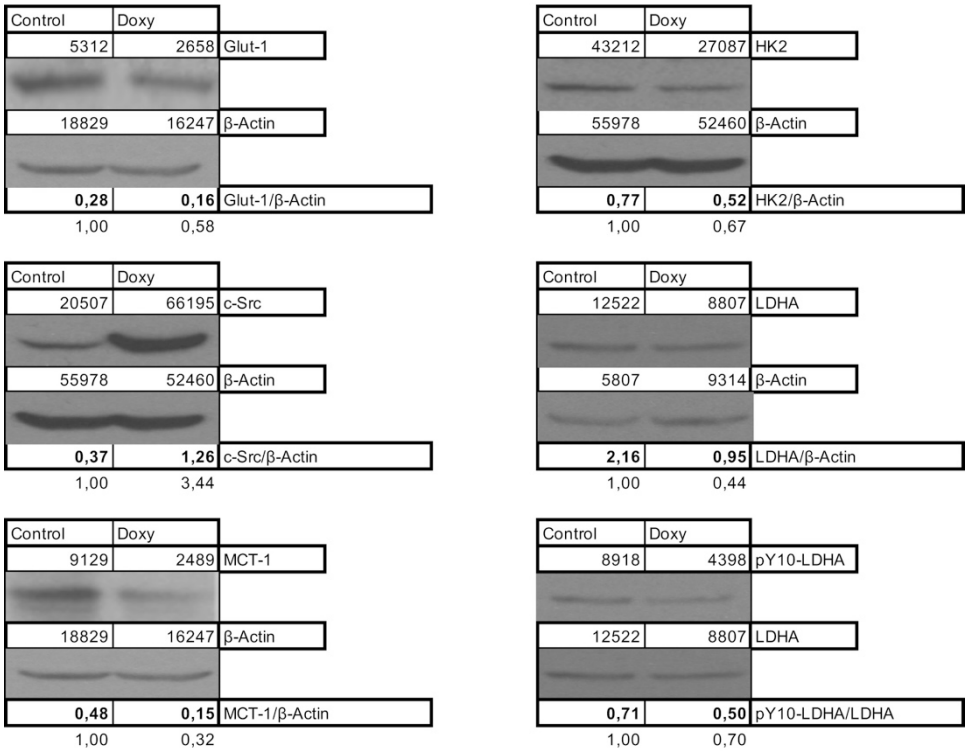

MCF7-Tet-On-SrcDN Mammospheres (FIGURE S8)

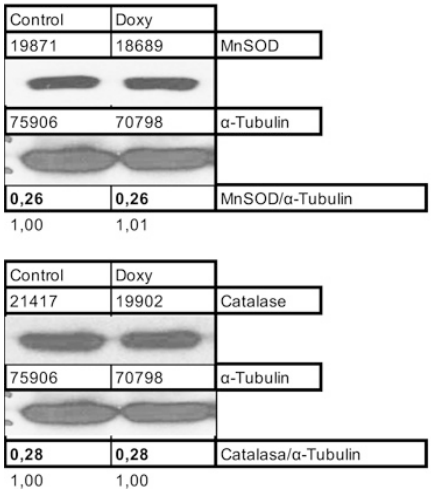

2.13. Quantification of immunoblots.

3. References

1. Cruz-Bermudez, A.; Vallejo, C.G.; Vicente-Blanco, R.J.; Gallardo, M.E.; Fernandez-Moreno, M.A.; Quintanilla, M.; Garesse, R. Enhanced tumorigenicity by mitochondrial DNA mild mutations. *Oncotarget* **2015**, *6*, 13628-13643, doi:10.18632/oncotarget.3698.